3-1954

Radioactive disintegration spectra of some short-lived nuclides

Warren A. Hunt
Iowa State College

D. J. Zaffarano
Iowa State College

Radioactive disintegration spectra of some short-lived nuclides

Abstract
The beta endpoint energies of several short=lived, low Z radioactive nuclides have been measured with an improved scintillation spectrometer. These values have been combined with recent half-life determinations to give the ft values.

Keywords
Ames Laboratory

UNITED STATES ATOMIC ENERGY COMMISSION

ISC-469

RADIOACTIVE DISINTEGRATION SPECTRA OF SOME SHORT-LIVED NUCLIDES

By
Warren A. Hunt
D. J. Zaffarano

March 1954

Ames Laboratory
Iowa State College
Ames, Iowa

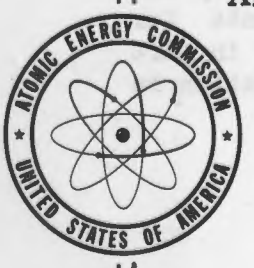

Technical Information Service, Oak Ridge, Tennessee

Subject Category, PHYSICS.
Operated by the Institute for Atomic Research of Iowa State College for the U. S. Atomic Energy Commission under Contract No. W-7405-eng-82.

F. H. Spedding: Director, Ames Laboratory

RADIOACTIVE DISINTEGRATION

SPECTRA OF SOME SHORT-LIVED NUCLIDES[1]

Warren A. Hunt and D. J. Zaffarano

ABSTRACT

The beta endpoint energies of several short-lived, low Z radioactive nuclides have been measured with an improved scintillation spectrometer[2]. These values have been combined with recent half-life determinations to give the ft values.

Table 1. Endpoint Energies, Half-lives, and ft Values for Some Superallowed Transitions.

Nuclei	Endpoint (Mev)	Half-life (seconds)	ft (seconds)
Mg^{23}	2.95 ± 0.07	10.7 ± 0.7 [3]	3600 ± 500
Si^{27}	3.76 ± 0.08	4.05 ± 0.10 [3]	4000 ± 450
S^{31}	4.50 ± 0.10	2.40 ± 0.07 [3]	5150 ± 600
Ca^{39}	6.10 ± 0.15	0.90 ± 0.05 [4]	7250 ±1000
Cl^{34}	4.45 ± 0.10	1.58 ± 0.05 [5]	3000 ± 400
K^{38}	5.06 ± 0.11	0.95 ± 0.03 [5]	3300 ± 400
P^{30}	3.31 ± 0.07	150 [6]	

[1] This report is based on a Ph.D. thesis by Warren A. Hunt submitted March, 1954 at Iowa State College, Ames, Iowa. This work was performed under contract with the Atomic Energy Commission.

[2] W. A. Hunt, W. Rhinehart, J. Weber, D. J. Zaffarano, Ames Laboratory Report ISC-359 (1953); to be published by the Rev. Sci. Instr.

[3] P. L. Phipps, The Half-lives of Some Short Lived Low Z Nuclei Formed by Photonuclear Reactions, Unpublished M. S. Thesis, Ames, Iowa, Iowa State College Library, 1953.

[4] R. Kline, Ames, Iowa, Preliminary Investigation, (Private communication) 1953.

[5] P. Stahelin, Phys. Rev. 92, 1076 (1953).

[6] L. N. Ridenour and W. J. Henderson, Phys. Rev. 52, 889 (1937).

For the group of superallowed transitions, the ft values times $|J|^2$, [7] increase with mass.

The ratio of gamma-ray intensity above 0.6 Mev to the intensity of the 0.51 Mev annihilation peak was less than two per cent.

A 15 per cent resolution at 624 kev was obtained with the anthracene crystal and photomultiplier tube. The linearity of the scintillation pick-up and recording equipment was tested with the 1.70, 2.24, 4.45, and 13.4 Mev beta endpoints of P^{32}, Y^{90}, Cl^{34}, and Li^{8}, respectively.

The targets, calibration system, and master control system which are used with the improved scintillation spectrometer are described. The control system automatically cycled the synchrotron, target and recording system until a sufficient number of events to yield the desired statistical accuracy had been obtained. Seventy discrete channels of information were obtained with the multichannel analyzer[2].

I. INTRODUCTION AND LITERATURE SURVEY

The purpose of this investigation was to determine the beta energy endpoints of some of the mirror nuclei which can be produced by the Iowa State College 70 Mev synchrotron. An improved scintillation spectrometer (1) permitted the attainment of much better statistical and calibration accuracies, and thereby better endpoint determinations than those obtained by previous investigators (2).

The mirror nuclei considered here are those pairs of nuclei with $|N - Z| = 1$ where N and Z are the number of neutrons and proton, respectively in these nuclei. The beta endpoints of these are of special theoretical interest as will be indicated by the following paragraphs.

In formulating the general Fermi theory of beta decay (3), there are five permissible Lorentz invariant interaction forms. Much experimental and theoretical work has been done to determine which of these forms are necessary to describe the observed beta spectra, since this information should be of assistance in determining the nature of nuclear forces.

Fermi (4), in his original theory, selected one of these forms and obtained a set of selection rules called the Fermi rules. Gamow and Teller (5) showed that if another one of these forms was chosen it would better fit some of the existing data. The selection rules from this theory are called the Gamow-Teller or the G-T rules.

---

[7] O. Kofoed-Hansen, Phys. Rev. 92, 1075 (1953).

For comparison of the allowed spectra with experiment, the five forms can be combined into two terms, and the probability for decay, P(E), of an electron of energy E in an energy interval dE can be written as

$$P(E)dE = (m_o^5 c^4 / 2\pi^3 \hbar^7)\, F(E,Z)(E^2-1)^{\frac{1}{2}}\, E(E_o-E)^2 dE \times$$
$$\times \quad (G_F^2 \left| \int 1 \right|^2 + G^2_{G-T} \left| \int \sigma \right|^2)$$

where G_F and G_{G-T} are the Fermi and G-T coupling constants, respectively, E_o and E are the maximum beta energy and the energy of the emitted beta particle, respectively, in $m_o c^2$ units, Z is the nuclear charge of the daughter product, F is the Fermi function which corrects the observed electron energy for the effects of the Coulomb forces, m_o is the rest mass of the electron, c is the velocity of light, $\hbar$ is Planck's constant divided by 2π, and the absolute value squared integral terms are the Fermi and G-T type interaction terms. The terms in this equation can be integrated with respect to E and evaluated, and the result can be written as

$$ft\,(G_F^2 \left| \int 1 \right|^2 + G^2_{G-T} \left| \int \sigma \right|^2) = \text{constant}$$

where t is the half-life of the transition and f is a dimensionless integral which corrects the observed half-life for the effects of the nuclear Coulomb field and the energy distribution of the transition. The unknowns in this equation are the terms in the parenthesis.

Wigner (6), on the basis of his supermultiplet model, first calculated the integral squared terms for the mirror nuclei and those nuclei with two odd nuclei over an even core of N = Z. Moszkowski (7) was the first to use the second equation to evaluate the ratios of the G's for these transitions. Trigg (8) made a detailed analysis using all the available data on the superallowed transitions and obtained a value of $(G_F/G_{G-T})^2$ of 0.5. Winther and Kofoed-Hansen (9) plotted the equation

$$B = ft \left[(1 - x) \left| \int 1 \right|^2 + x \left| \int \sigma \right|^2 \right]$$

for the mirror nuclei and those nuclei which have closed shells in both neutrons and protrons plus or minus one particle, where x equals

$$G^2_{G-T} \Big/ \left(G_F^2 + G^2_{G-T} \right) .$$

They obtained a value for B of 2600 $\pm$ 85 and for x of 0.50 $\pm$ 0.05.

The values of the integrals in the equation for B have been calculated for the superallowed transitions using various nuclear models and are listed for several nuclides in the papers of Wigner, Trigg, and Winther. If the data were consistent with a single value of x and B for a particular nuclear model, very strong support for this model

would be obtained and the interaction strength constants, the G's, could be calculated.

A large part of the uncertainties in the x and B are due to the uncertainties in the ft values used in the calculations. The purpose of this investigation was to obtain a better determination of the beta endpoint energies for the mirror transitions and thereby the f values. The f values found are combined with the best available $t_{\frac{1}{2}}$ values in Table 3.

II. EQUIPMENT, TESTS, AND ERRORS

Description of Equipment

A description of the equipment used in this investigation has been published as ISC-359 (1). Further description will be given of only the components not covered in that report. These are the cycle control circuit, the target transport system, the targets, and the scintillation pickup.

In order to produce enough activity in the element being investigated, it was necessary to have the target sample close to the "donut" of the synchrotron, since a thin target was used in order to minimize the energy loss of the electrons as they were emitted during radioactive decay. It also was necessary to have the photomultiplier tube used in the spectrometer at such a distance from the synchrotron that the synchrotron's magnetic field would not interfere with the operation of the tube. This was achieved by the fast pneumatic target transport system which was controlled by the cycle programming equipment.

The transport system consisted of a rectangular aluminum tube about ten feet long with one closed and one open end. A block of balsa, to which the target was attached by means of a nickel frame, was formed so that it would slide freely in the tube. A pipe was attached to the closed end of the tube so that by applying either more or less than atmospheric pressure to the pipe, the target could be made to rapidly move to either end of the tube, i.e.; to the bombard or the record position. When the target was in the record position, the radioactive sample protruded from the end of the tube and was positioned accurately parallel to the scintillation crystal and about $\frac{3}{4}$" away.

All of the targets for the beta spectra except magnesium, silicon, and beryllium were prepared by pressing powder into a thin wafer with pressures of 5000 lb/in^2. The wafers were 1.165 inches in diameter and less than 50 mg/cm^2 in thickness. The thickness was checked by weighing

the samples after pressing. Those that were too heavy were discarded. The acceptable samples were then mounted with diluted Duco cement between two sheets of rubber hydrochloride which had a thickness of 0.5 mg/cm^2. The rubber hydrochloride was cemented to a rigid, light weight nickel frame which in turn was fastened to the balsa wood block mentioned previously. The Silicon target was prepared by spreading over the same area enough powder to give it the desired thickness. It was bonded similarly. The magnesium target was prepared from strips of metal such that is presented a target one inch square by 0.005 inches in thickness. The beryllium target was similar to the magnesium one, except it was a solid sheet one inch square by 0.005 inches. The constituents of the targets will be listed as they are discussed under the name of the isotope.

In order to obtain enough counts per channel for good statistical accuracy, it was necessary to bombard and record many times. This was facilitated by the automatic control equipment (Figure 1) which cycled the synchrotron and the recording equipment. The following operations comprised one cycle:

1. The target was in bombard position with the synchrotron ON and the recording equipment OFF;

2. The target was in transit from the bombard position to the record position with the synchrotron OFF and the recording equipment either OFF or ON as desired;

3. The target was in record position with the synchrotron OFF and the recording equipment ON;

4. The target was in transit from the record position to the bombard position with the synchrotron OFF and the recording equipment OFF.

The time of each of these operations could be varied as desired. The usual procedure was to have the duration of operations 1 and 3 equal two half-lives. The transit time, step 2, could be varied from less than one-half to three seconds, with one second being the usual time. The time for step 4 could be varied from three to twelve seconds. The only long lived activity that interfered with the shorter half-life measurement was the 2.5 minute activity of P^{30} in the phosphorus sample.

The time required to run a calibration and the unknown spectrum varied from two to five hours. For these periods the equipment was as stable and drift-free as the equipment used for testing, which was reliable to one-half of one per cent.

The scintillation pickup consisted of an anthracene crystal and

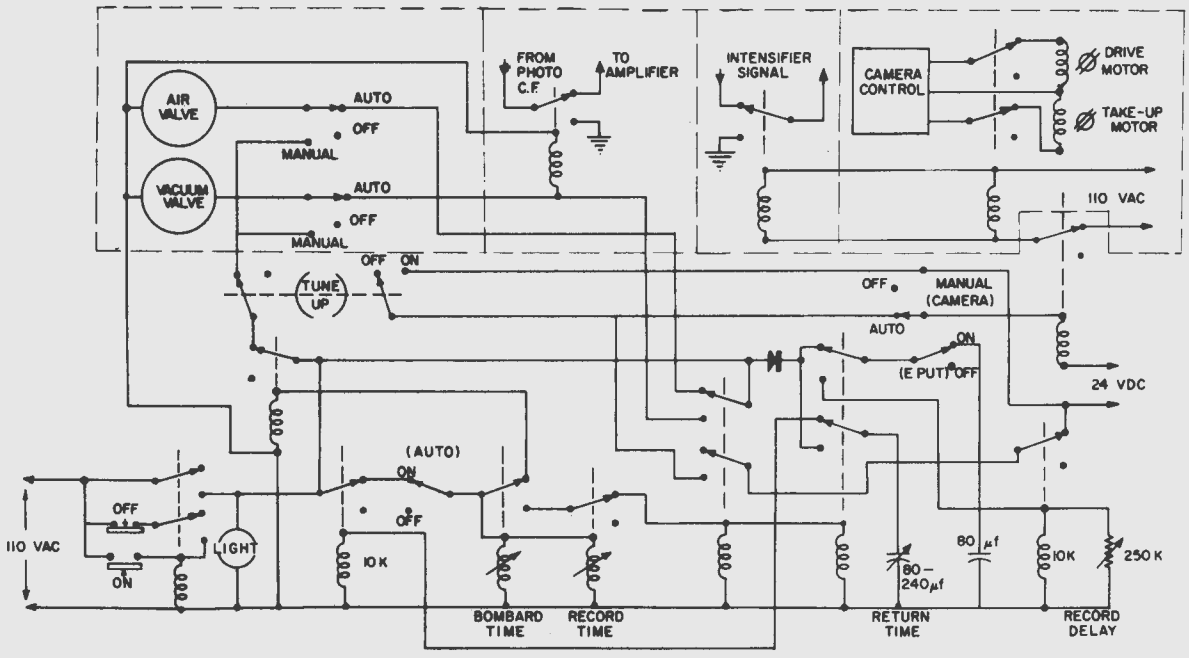

Figure 1. Circuit Diagram of the Automatic Cycle Control.

photomultiplier tube, a cathode follower, a pulse generator, and a step attenuator.

A typical scintillation crystal and phototube mount is shown in Figure 5, page 13 of Phipp's thesis (10) with the exception that no MgO coating was used on the top 3.1 mg/cm^2 aluminum reflector through which the beta-rays entered the crystal. A resolution of 15 percent with a peak to valley ratio of three to one was obtained with the Cs^{137} internal conversion line. This was consistent with the resolution reported by Phipps. These data were taken with a 1.5 inch crystal mounted on a Dumont 6177 photomultiplier tube, and also with Boley's (2) one inch crystal mounted on an RCA 5819 tube. Tests to determine the energy lost by electrons in transversing the 3.1 mg/cm^2 aluminum reflector indicated that the displacement of the apparent maximum of the 624 kev internal conversion electron peak of Cs^{137} is less than 10 kev. These tests were carried out by scanning the cesium 137 conversion peak after placing zero through five 3.1 mg/cm^2 additional aluminum sheets between the source and the crystal.

The photomultiplier, step attenuator, and cathode follower circuit diagram is shown in Figure 2. The voltage pulse for a single event had a total duration of about two microseconds. This was determined by the capacity of the collector anode plus the input capacity of the cathode follower and the grid resistor. A pulse of nearly the same shape was produced by a simple pulse generator and was applied to the input of the cathode follower after attenuation by the decade resistor network.

The step attenuator was made with precision resistors mounted on an eleven position stepping relay. This type relay was selected in order that it could be mounted beside the cathode follower and be controlled remotely. As shown in Figure 2, the step attenuator could be disconnected from the cathode follower by pushing the RESET button. In order to eliminate electrical noise from the synchrotron, the pulse generator and the step attenuator control power cable were also disconnected while data were being taken.

In addition to the tests of the equipment reported in ISC-359, additional checks of the linearity of the scintillation pickup and the remainder of the equipment were made by determining the beta-endpoints of P^{32} (11), Y^{90} (11), Cl^{34} (12), and Li^{8} (13). The results of these runs, Figures 3,4,11,12,21, and 22, show that the equipment was linear to 13 Mev in agreement with the step attenuator calibration procedure.

Experimental Procedure and Calibration

The camera used for recording the pulse information displayed on the oscilloscope was designed for only 100 feet of film at a loading.

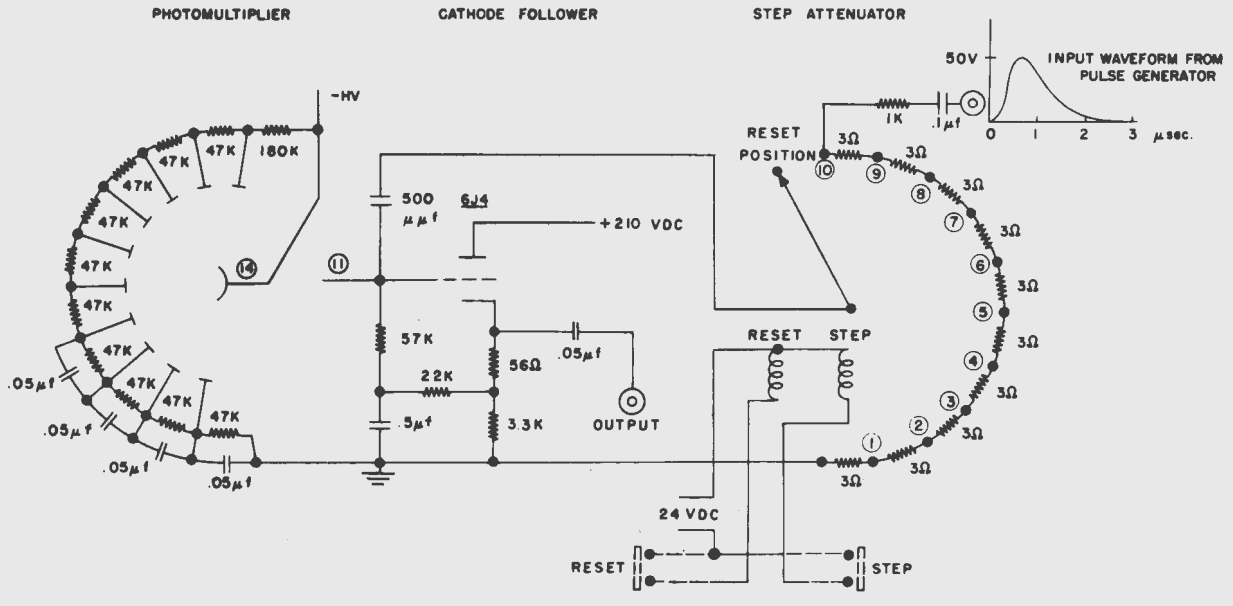

Figure 2. Circuit Diagram of the Scintillation Pick-up.

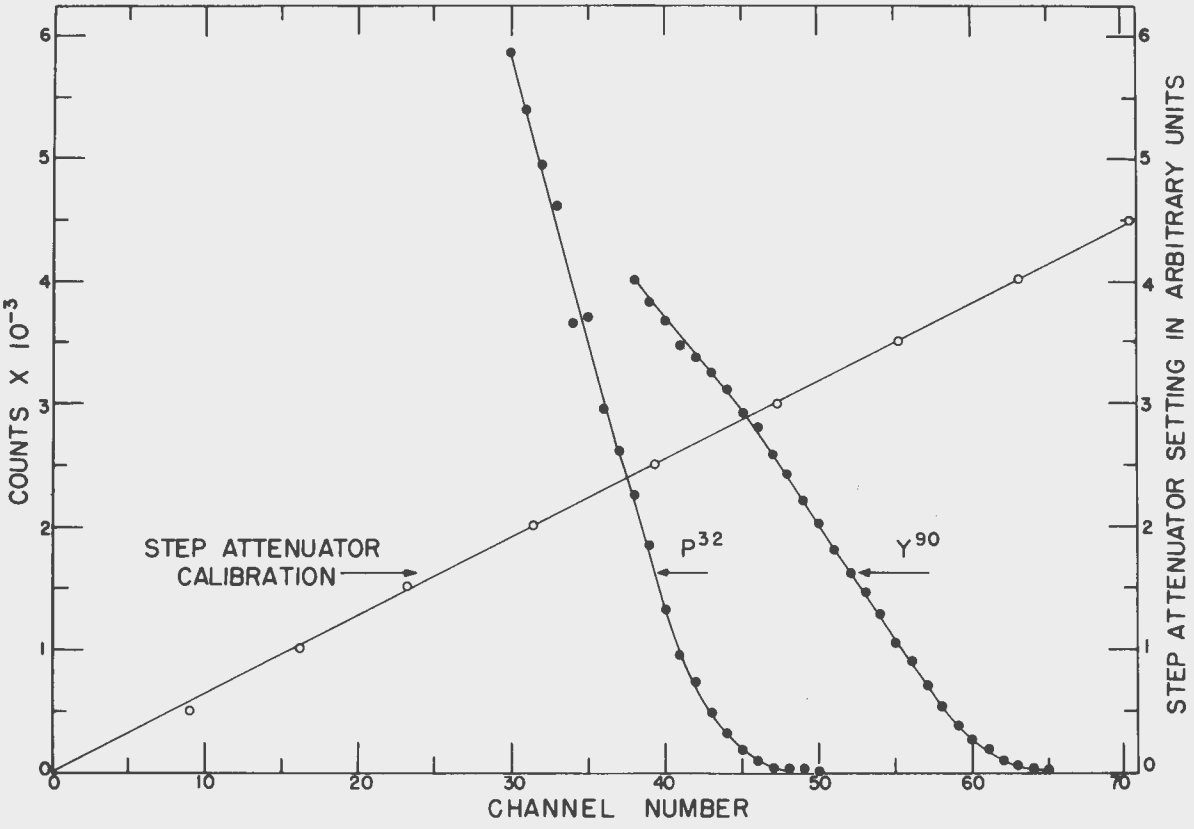

Figure 3. Beta Spectra of P^{32} and Y^{90}.

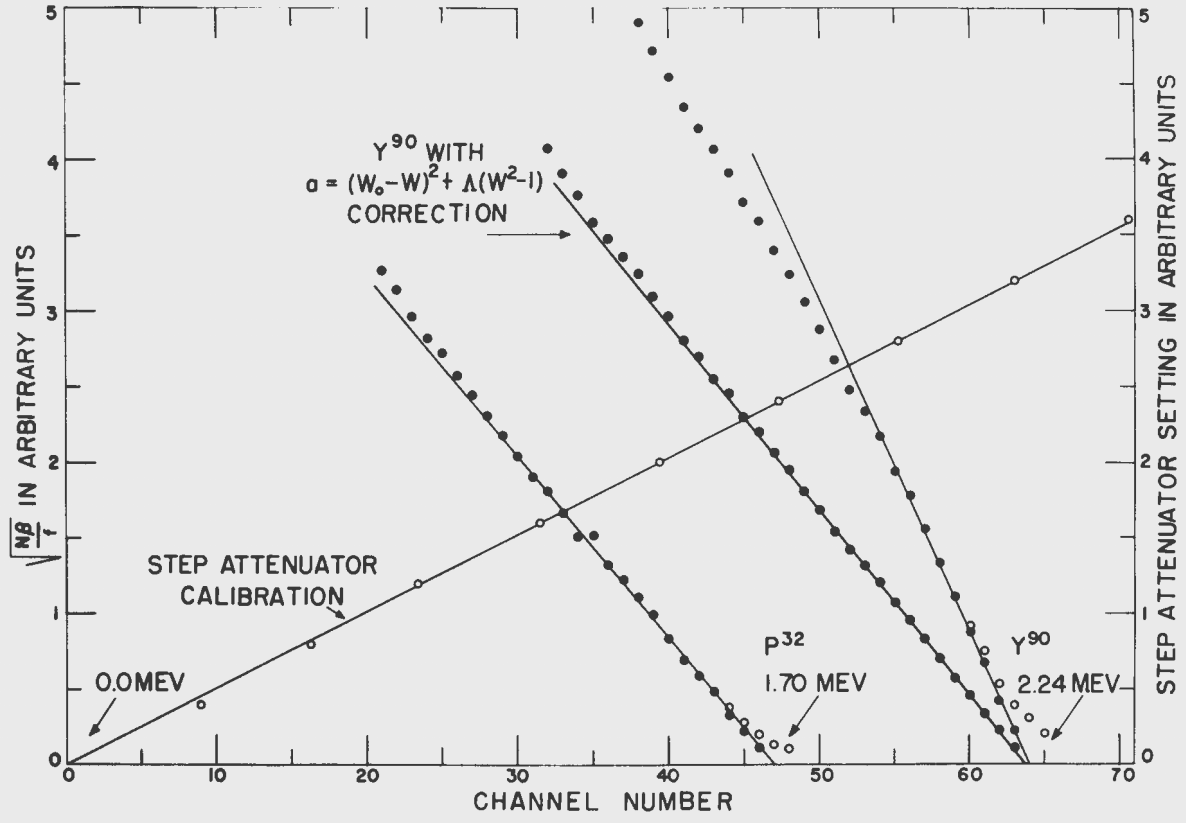

Figure 4. Kurie plots of P^{32} and Y^{90}.

Since it was not practical to reload the camera with the assurance that the position of the camera with respect to the oscilloscope had not been changed, a run was concluded when 100 feet of film had been used. This was enough to obtain good statistical accuracy of the calibration and the unknown spectra.

The procedure used in all cases in which Cl^{34} served as a calibration spectrum was to bombard an unmounted NH_4Cl wafer for one hour and then to place it on the top alluminum reflector of the scintillation tube and crystal. In order to obtain the desired number of events from Cl^{34}, it was necessary to record for about 30 minutes and to use about 40 feet of film. Next, a linearity calibration was recorded from the pulse generator and step attenuator. As an added check, about 10 or 15 feet of Y^{90} was recorded with such a film speed as to yield a high density of dots near the endpoint of the spectrum. The remainder of the 100 feet of film was used to record the activity of interest.

The film was developed and processed through the multichannel analyzer as described in ISC-359.

The data obtained from the automatic film scanner were number of counts and step attenuator positions versus the channel number. The channel number scale is later converted to an energy scale. These results are shown, with the exception of Figure 1 and 6, as the odd numbered figures. When the positions of the step attenuator versus the channel numbers at which the calibration pulses appear are plotted, the nonlinearity of the equipment shows up as the deviation from the straight line. As can be seen, the equipment was linear within experimental error except at either end. This nonlinearity is due at the lower end to the nonlinear resistances of the crystal diodes in the clipping circuit, and at the upper end to the nonlinear charachteristic of the oscilloscope for large deflections. By keeping the pulse sizes within the linear range of the equipment, the position of the "baseline" or zero pulse amplitude could be obtained by extrapolation of the calibration curve. That this zero was the true zero within experimental error was verified by the linearity experiments. The baseline can also be inferred from the statement by Birks (14) that if the voltage pulse height from an anthracene photomultiplier spectrometer is plotted versus energy for the electrons stopped by the crystal, the plot is linear above 125 kev and the linear portion, if extrapolated, crosses the energy axis at plus 25 kev. For most of the figures, 25 kev is of the order of one dot radius, hence the zero correction for any saturation effect is probably negligible.

With the zero amplitude "baseline" determined, it is necessary to determine the energy of at least one other point in the linear region of the equipment in order to have an energy calibration. For most of the data, the 4.45 Mev (12) beta-ray endpoint of Cl^{34} and the 2.24 Mev (15) endpoint of Y^{90} were used. The Y^{90} served as an additional check

when it was used with the Cl^{34}.

The endpoints were determined by making a Kurie plot from the spectrum. The Kurie plot consists of plotting the function $\frac{N\beta}{f}$ versus the energy where N is the number of counts at a given energy, β is the ratio of the velocity of the electron to the velocity of light, and f is the modified Fermi function as given in the National Bureau of Standard's Tables for the Analysis of Beta Spectra, Applied Mathematics Series, No. 13. In the following graphs, N is the number of counts at a given channel number.

Because f is a function of nuclear charge and energy, an energy scale must be assumed before a calibration Kurie plot can be made. This was done by selecting a suitable channel number from inspection of the observed spectrum and assigning to it the known endpoint energy. A Kurie plot was made with this assumption and a new channel number endpoint determined. This new endpoint was used for the next Kurie plot. This process converged rapidly to a unique endpoint.

An examination of the Kurie plots will show a fairly long straight portion near the end with the points bending up from the straight line at either end. The bending near the endpoint is caused by the resolution spread of the instrument. Calculations which make corrections possible have been made by Palmer and Laslett (16). With the exception of P^{30} (Figure 14) the uncorrected points show on the Kurie plots as open circles and the corrected points as solid dots below each of the open circles.

In making these corrections, it was necessary to know the resolution of the instrument at the energy at which the correction was being made. This was obtained for any energy by measuring the resolution for the Cs^{137} conversion line and using the fact that the resolution is known to go inversely as the square root of the energy.

Because of the bending of the Kurie plots at lower energies, several tests were run on Cl^{34}, Y^{90}, and P^{32} to determine over what portion of the spectrum the Kurie plots could be relied upon for endpoint determinations. Figure 4 shows the result of one such test. This may be compared with some of the Cl^{34} calibration Kurie plots. These Kurie plots and the Kurie plot of Li^{8} indicate that an allowed spectrum will give a straight Kurie plot for about the upper one-third of the spectrum from 2 to 13 Mev, when a scintillation counter is used as a detector.

In an attempt to determine the cause of this bending, the spectra shown in Figures 5 and 6 were run. The chlorine 34 sources were extracted by the Szilard-Chalmers (17) process from a bombarded volume of CCl_4. The activity was deposited upon a 3.1 mg/cm^2 aluminum backing and placed three inches from the top of the crystal and on the axis of symmetry of the

tube and crystal. There were four runs of 50 feet of film each. In the first run, a lead shield three eighths of an inch thick with a one-half inch hole was placed so that the shield was one inch from the top of the crystal and the hole was on the axis of symmetry of the system. In the second experiment the lead shield was removed and a lead cylinder three-eighths of an inch high and one-half an inch in diameter was placed in the position occupied by the hole. This was accomplished with the use of a sheet of 0.5 mg/cm^2 rubber hydrochloride which was also in place when the first run was made in order to have identical energy losses outside of the crystal. The third experiment was like the first except that the lead was replaced with aluminum. The fourth experiment was with no shield of any type.

In the spectra obtained with the lead cylinder versus the hole (Figure 5) it can be seen that the number of counts at a given energy for the cylinder is less than the number with the hole for high energies and is greater for low energies. This indicates that loss of electrons through the edges of crystal caused some of the high energy electrons to be counted as low energy electrons which, in turn, caused the Kurie plot to bend upward at lower energies. The rapid turn up at about channel 34 is caused by a second beta group in Cl^{34}.

Because of the small solid angle permitted with the hole and the weak activities of the targets, it was not possible to use this method to straighten the Kurie plots.

Errors in Endpoint Determinations

The probable errors quoted with the beta endpoint energies are due to the uncertainties in the calibration energies, the zero energy point, and the endpoint channel numbers determined from the Kurie plots for both the calibration and unknown spectra.

As mentioned previously, a zero energy point could be determined by the use of a calibrated step attenuator. The probable error in each step attenuator calibration point is about the radius of the dot. The zero point was obtained by extrapolating the linear portion of the step attenuator setting versus channel number until the channel number axis was intersected. This zero had a probable error of less than one-half of a channel. One-half channel was used for error calculations.

Both Y^{90} and Cl^{34} have been measured by magnetic spectrometers, but the errors in the quoted endpoints are large enough that they must be considered in determining the probable errors in these measurements. The reported endpoints for Y^{90} are 2.27 $\pm$ 0.02 Mev (18), 2.25 Mev (19), 2.24 Mev (20), 2.23 Mev (21), and 2.18 $\pm$ 0.007 Mev (22). From these values, a value of 2.24 $\pm$ 0.04 Mev was assigned to Y^{90} for calibration purposes. The Cl^{34} endpoint has been measured as 4.45 $\pm$ 0.11 Mev (12) and 4.46 Mev (23). From these values, together with the values resulting from

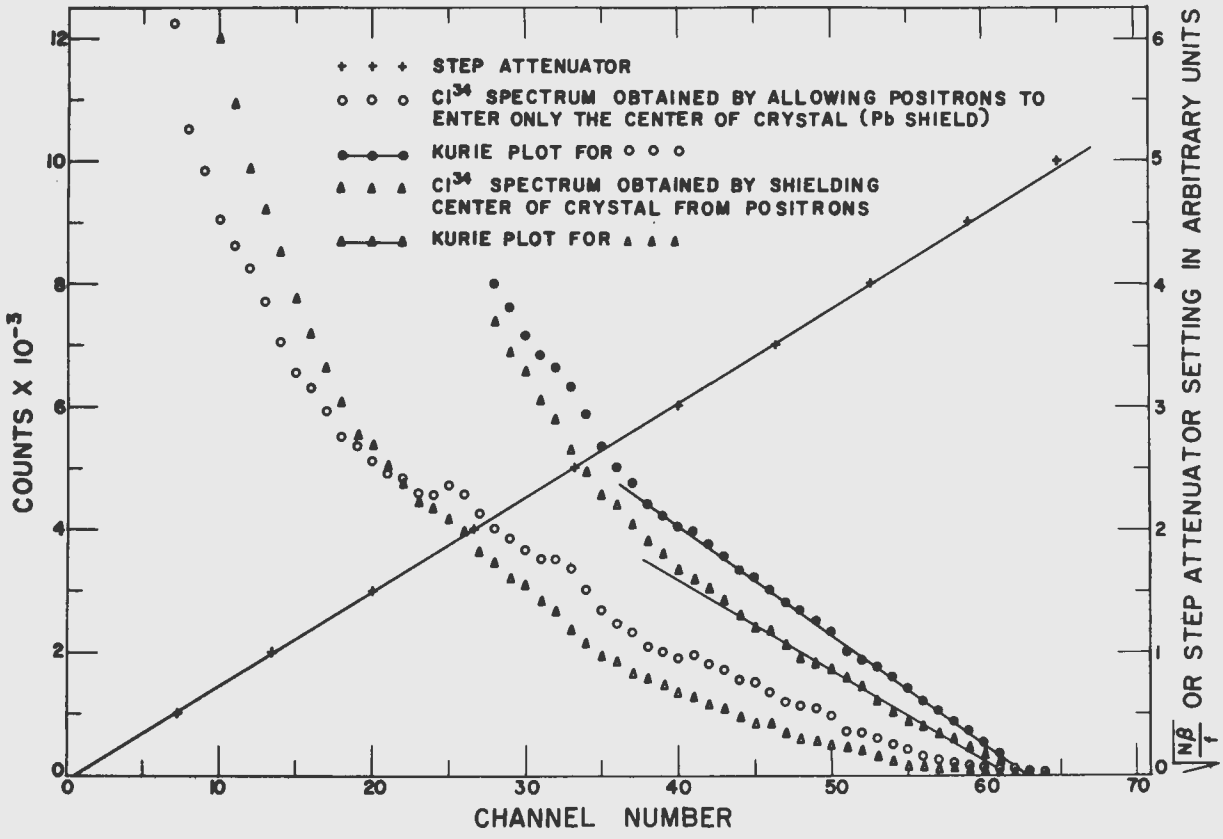

Figure 5. Results of Tests to Determine the Effect Caused by Electrons Which Enter the Edge of the Crystal.

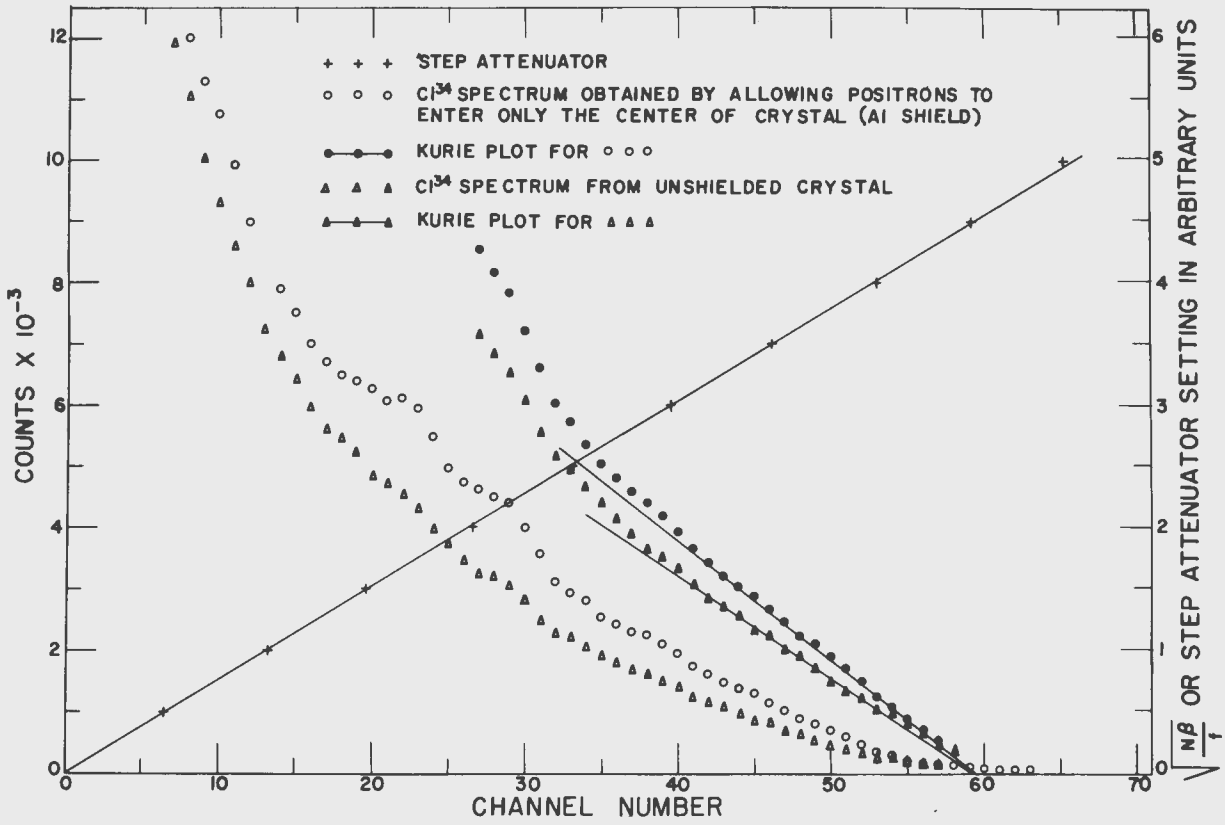

Figure 6. Results of Comparing the Crystal with No Shield to the Crystal with the Edges Shielded.

repeated comparisons of Cl^{34} and Y^{90} in this investigation, an end point value of 4.45 ± 0.10 Mev was assigned to Cl^{34}.

In addition to these errors, additional errors were introduced in determining the endpoints from the Kurie plots. To determine the endpoint, only the high energy straight section of each Kurie plot was used. In order to determine what portion of the Kurie plot was the straight section, a straight edge was used to connect as many dots as possible, with an allowable deviation of one dot diameter. Then, a least squares best fit was made to the points along this region. The probable error from this method was not more than one-half of one channel. One-half channel was used as the probable error for calculations.

The quoted probable error, e_n, for the unknown endpoint energy, E_n, will be defined for the case of n calibration points. Let E_i, $i = 0,1,2,\cdots, n-1$, be the n energy calibration points; V_i be the channel numbers corresponding to these points; E_n and V_n be the unknown energy and channel number, respectively; e_i and v_i be the probable errors in E_i and V_i, $i = 0,1,2,\cdots,n$, respectively; and A and K be constants to be determined. Since the equipment was linear,

$$E_i = K(V_i - A).$$

To make a least squares best fit, the function

$$\sum_{i=o}^{n-1} \left[E_i - K(V_i - A) \right]^2$$

is minimized with respect to K and A. K and A can be determined in terms of the E_i and V_i. Then E_n can be found as a function of the E_i, $i = 0,1,2,\cdots, n-1$, and the V_1, $i = 0,1,2,\cdots,n$ from the relation

$$E_n = K(V_n - A).$$

The probable error e_n is defined as

$$e_n \equiv \left[\sum_{i=o}^{n} \left(\frac{\partial E_n}{\partial V_i} v_i \right)^2 + \sum_{i=o}^{n-1} \left(\frac{\partial E_n}{\partial E_i} e_i \right)^2 \right]^{\frac{1}{2}}$$

The error determined in this manner agreed very well with that observed in the repeated runs of Cl^{34} and Y^{90}. A further check was

furnished by the several determinations of each unknown. From the close grouping of values in Table 1 for each unknown determination, it can be seen that the uncertainties in the energies of the calibration points represent a large fraction of the probable error. The fraction of the probable error from this cause ranged from about one-third for Mg^{23} to one-half for Ca^{39}. If Cl^{34} and Y^{90} could be determined more accurately, these quoted errors could be reduced.

Discrepancies in the values reported here and others will be discussed under the isotope in question.

III. APPLICATIONS TO SOME SUPERALLOWED TRANSITIONS

Magnesium 23

Mg^{23} was formed by a (γ, n) reaction on stable Mg^{24}. The target was made from 0.005 inch foil. The longer half-life permitted the activity to be recorded with more ease than any of the other activities. For this reason, Mg^{23} was used to test the equipment. The three runs shown in Table 1 were made in July, August, and October. The two earlier runs were made with the one inch crystal used by Boley. The statistics of the October run, the results of which are shown in Figures 7 and 8, were better than those of the other two. Y^{90} was used as the calibration spectrum in all cases.

The three runs were averaged and the value of 2.95 ± 0.07 Mev was assigned to Mg^{23}. This agrees very well with the value by Boley and Zaffarano of 2.99 ± 0.10 Mev and the 2.8 Mev cloud chamber measurement (24). Except for a possible very weak high energy tail in the October run, there was no evidence for another beta group.

The agreement with Boley in this case and the disagreement in the other cases can be explained in part by the fact that no other beta transition is apparently excited by 70 Mev x-ray bombardment. Since no other noticeable beta group existed, Boley's assumed endpoint, which was probably based on an extrapolation of the straight portion of the Kurie plot to the energy axis, was the correct endpoint within experimental error. Discussions of the effects of a second beta group are made under the isotopes with which a second beta group was observed.

Silicon 27

Si^{27} was formed by a (γ, n) reaction on Si^{28}. The target was of silicon powder better than 97 per cent pure with the greatest impurity being iron at 1.5 per cent maximum. Figures 9 and 10 show the

Table 1. Beta Endpoint Energies for Various Runs.

Nuclei	Endpoint (Mev)	Bomb. Energy (Mev)	Crystal thickness (inches)	Calibration beta spectra
Mg^{23}	2.98	65	1	Y^{90}
Mg^{23}	2.93	25	1	Y^{90}
Mg^{23}	2.95	65	1½	Y^{90}
Si^{27}	3.73	30	1	Y^{90}
Si^{27}	3.76	65	1	Y^{90}
Si^{27}	3.76	65	1½	Y^{90}
Si^{27}	3.78	65	1½	Cl^{34}, Y^{90}
P^{30}	3.30	65	1½	Cl^{34} , Y^{90}
P^{30}	3.32	65	1½	Cl^{34} , Y^{90}
S^{31}	4.45	65	1½	Y^{90}
S^{31}	4.38	65	1	Y^{90}
S^{31}	4.50	65	1½	Cl^{34} , Y^{90}
S^{31}	4.52	65	1½	Cl^{34}
Cl^{34}	4.44	65	1	Y^{90}
Cl^{34}	4.45	65	1½	Cl^{34}
K^{38}	4.95	65	1	Y^{90}
K^{38}	5.00	65	1½	Cl^{34} , Y^{90}
K^{38}	5.10	65	1½	Y^{90}
K^{38}	5.10	65	1½	Cl^{34} , Y^{90}
Ca^{39}	6.10	65	1½	Cl^{34} , Y^{90}
Ca^{39}	6.00	65	1½	Cl^{34} , Li^{8}
Ca^{39}	5.95	65	1½	Y^{90}
Ca^{39}	6.15	40	1½	Cl^{34} , Y^{90}
Li^{8}	13.4	65	1½	Cl^{34}

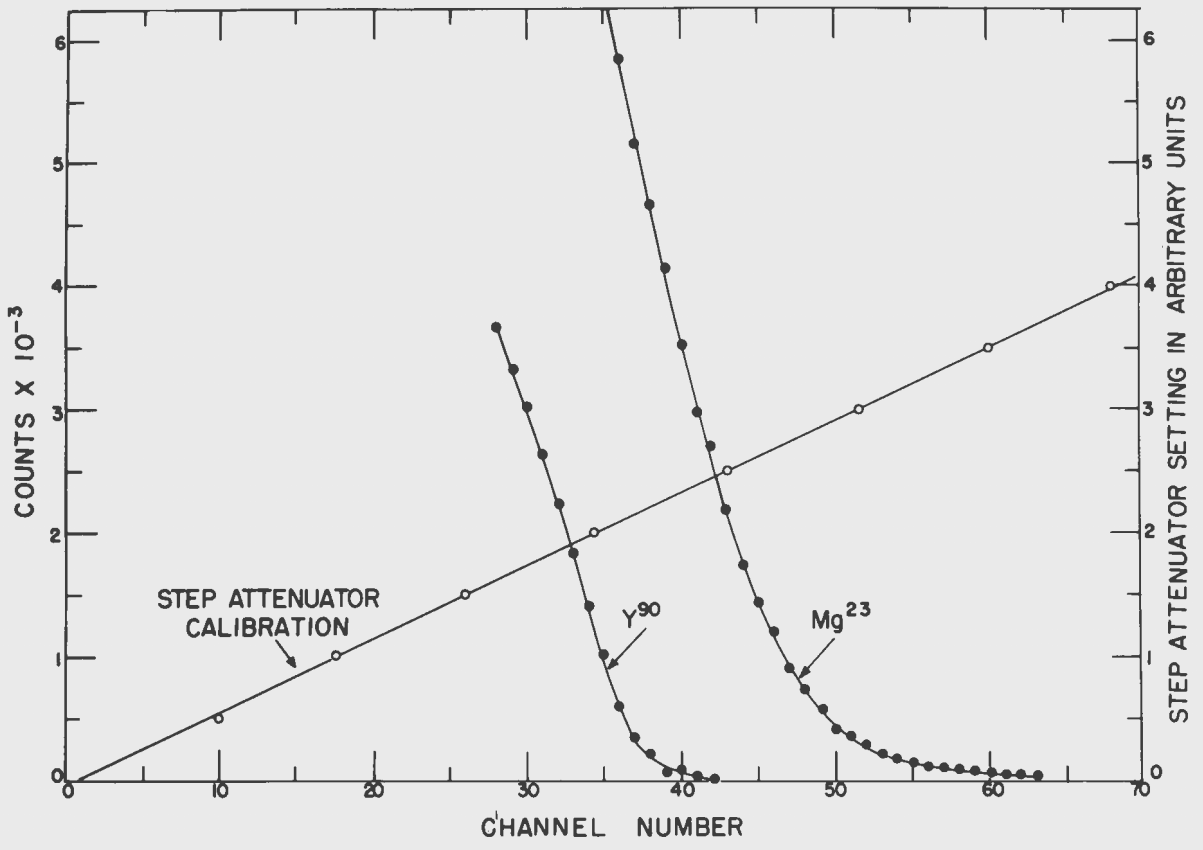

Figure 7. Beta Spectra of Mg^{23} and Y^{90}.

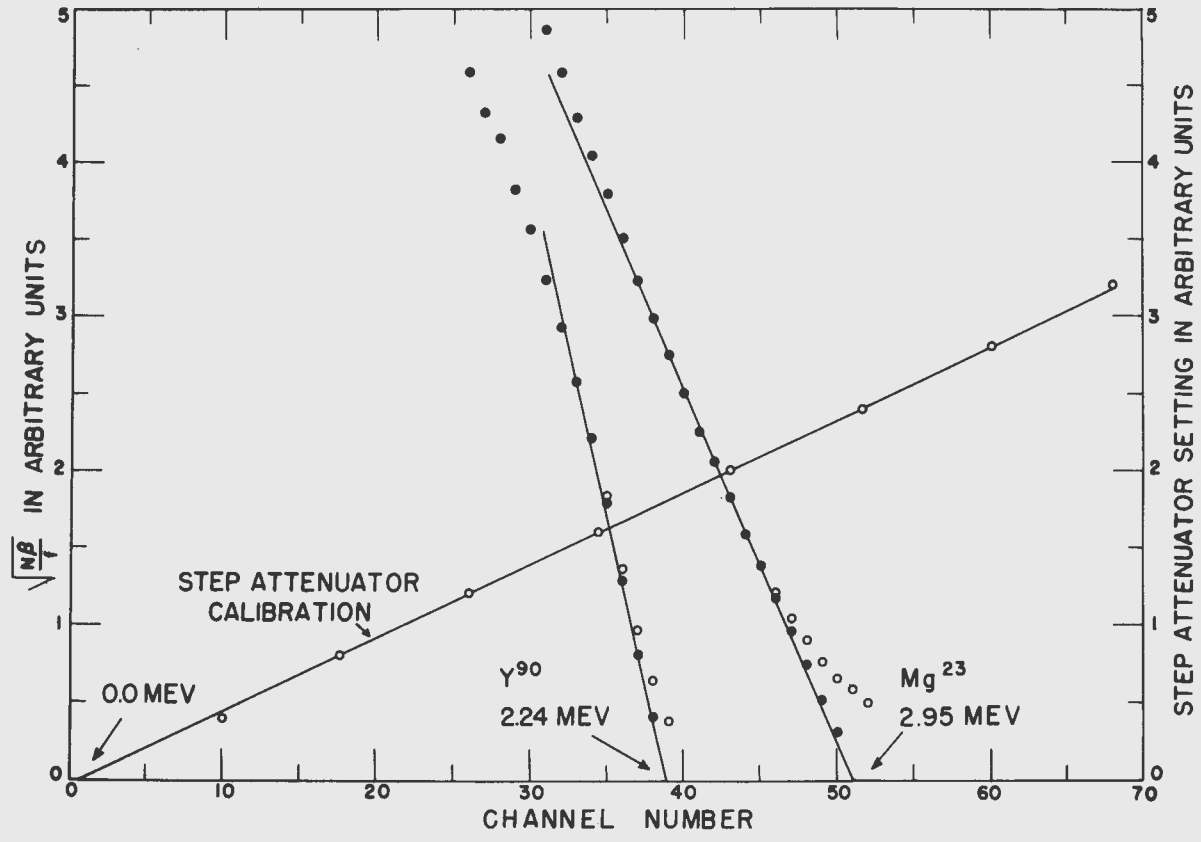

Figure 8. Kurie Plots of Mg^{23} and Y^{90}.

results of one of the four runs. Two of these runs were made under identical conditions with the exception that one was made with the synchrotron at 65 Mev and the other at 30 Mev maximum beam energy. The other two runs were made with the synchrotron at 65 Mev. The first two runs were recorded with Boley's one inch crystal mounted on an RCA tube, and the other two runs were recorded with the one and one-half inch crystal mounted on the Dumont tube. The results of these runs are given in Table 1.

A second beta group was noticed in each of these runs. A subtraction was done in the two cases which had the better statistics, and the endpoints of 3.1 and 3.2 Mev were obtained. An estimate was made of the relative recorded intensities of the highest energy beta group and the second group obtained by the subtraction process from the Kurie plot* The ratios were about two to one for the 65 Mev bombardment and about four to one for the 30 Mev bombardment. The amount of the second group as compared to the first increased when the bombarding time was increased from eight to ten seconds, the delay before recording increased from about one-half a second to one second, and the recording time in both cases kept at ten seconds. It is known that, in addition to the (γ, n) reaction, all other reactions that are energetically possible are probably produced to some extent. After the (γ, n) and the (γ, p) reactions, the (γ, np) and/or the (γ, d) reactions are the next most probable. Edwards and MacMillian (25) found some reactions were reduced in intensity by a factor of about ten compared to the (γ, n) reactions.

According to Kofoed-Hansen (26), Si^{26} should have an energy of 3.64 Mev and a half-life of 3.4 seconds. Since the higher energy beta group was the main group observed, especially at 30 Mev, and since the calculated threshold for the $(\gamma, 2n)$ reaction is 30 Mev, the higher energy group was assigned to Si^{27}. The preceding paragraph indicates that the 3.15 Mev beta group probably belongs to an activity with a longer half-life and a higher threshold than Si^{27}. All of the statements are consistent with assigning the 3.15 Mev group to Al^{26} which has reported values ranging from 2.8 to 3.4 Mev and a half-life of about seven seconds (27).

The value of 3.76 ± 0.08 Mev for Si^{27} was obtained by averaging the endpoint values of the four runs. Three of these were with Y^{90} as the calibration spectrum and the other was with Y^{90} and Cl^{34}. This is in fair agreement with the 3.48 ± 0.1 Mev value by Boley and the two cloud chamber measurements of 3.5 Mev (28) and 3.74 Mev (29).

If a straight line is extended from the 3.15 Mev beta group until it crosses the energy or channel number axis, the intersection is about 3.5 Mev. Since Boley did not suspect the presence of the second beta group, he corrected all points above the second beta group. These corrections had the effect of making the data agree with the endpoint assumption.

---

* For the method used, refer to the Appendix.

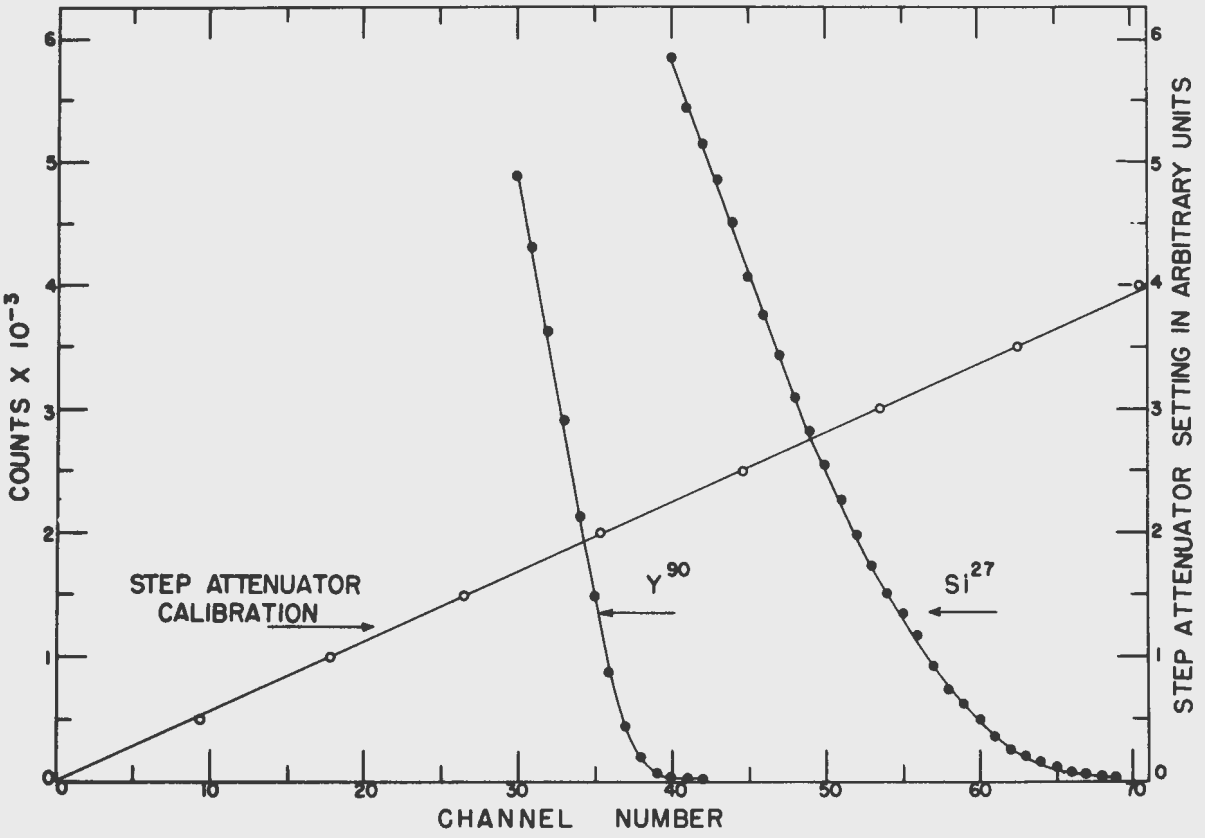

Figure 9. Beta Spectra of Si^{27} and Y^{90}.

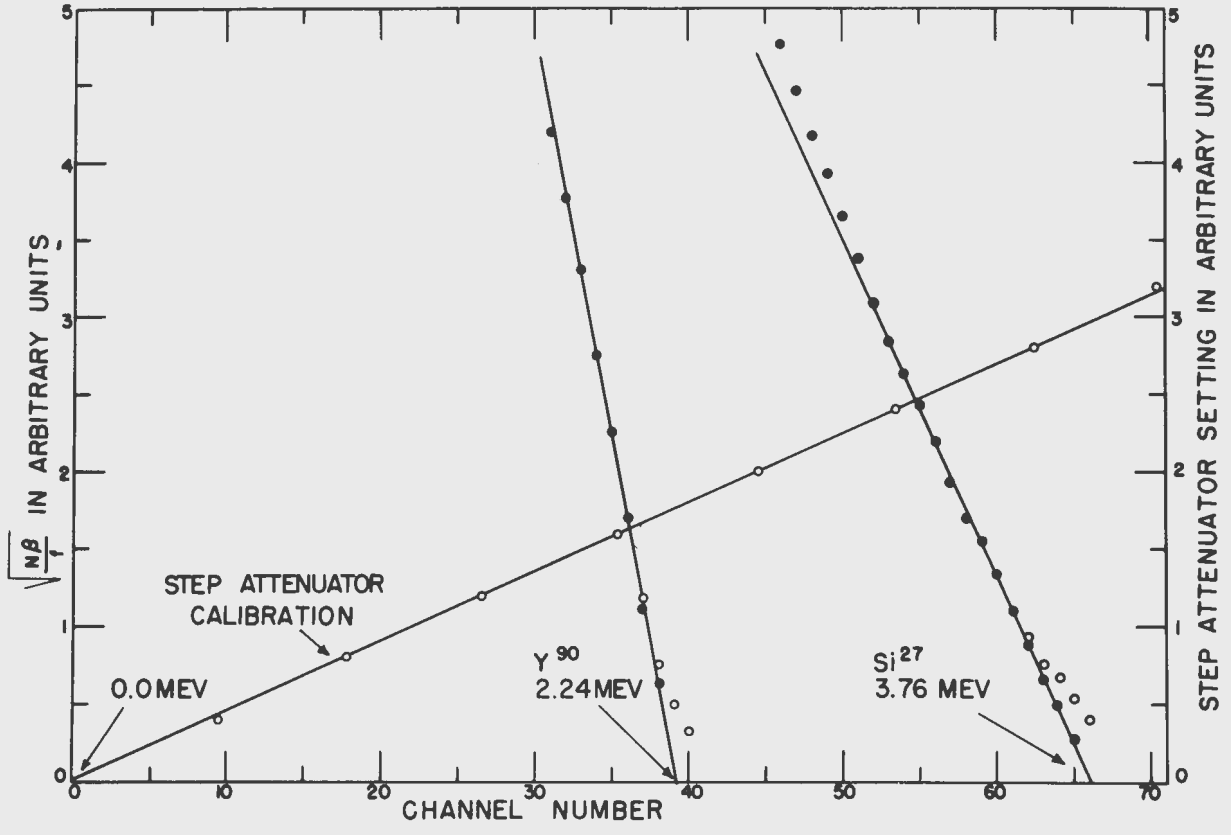

Figure 10. Kurie Plots of Si^{27} and Y^{90}.

Phosphorous 29 and 30

In order to produce P^{29}, it was necessary to obtain a $(\gamma, 2n)$ reaction on P^{31}. In addition to the P^{29}, P^{30} is produced. Usually, other activities can be ignored by energy or half-life considerations, but this was not so in this case. Since there were some discrepancies in the reported value of P^{30}, a spectrum of P^{30} was recorded and the Kurie plot made.

To obtain the P^{30} spectrum, P^{31} in the form of a pressed wafer of red phosphorous was bombarded for five minutes with the synchrotron at maximum energy and then allowed to decay for three minutes before the recording apparatus was started. Figures 11 and 12 show the spectrum and the 3.32 Mev value obtained from the Kurie plot.

P^{30} was produced in large quantities and a strong background of it built up in the attempt to run P^{29} giving another endpoint determination of 3.30 Mev for P^{30} (Figures 13 and 14). While this was not the result sought, it was very useful as a check on the first run. Due to the strong background of P^{30}, the P^{29} endpoint determination cannot be considered reliable. Since any value obtained by this method could not improve the accuracy of the 3.945 $\pm$ 0.010 Mev beta endpoint value (30), no further attempt was made to record the spectrum of P^{29}.

The assigned value of 3.31 $\pm$ 0.07 Mev for P^{30} is in fairly good agreement with the values of previous work. The value of 3.5 Mev was obtained with a spectrometer in 1941 (31). No experimental error was reported for this value. The 3.4 Mev value was obtained by absorption (32) and the 3.0 value with a cloud chamber (28).

Figures 13 and 14 serve as good examples of the difficulty of observing the $(\gamma, 2n)$ reaction over the (γ, n) reaction and, also, the effects of endpoint corrections. In Figure 14, the open circles along the lower portion of the line labelled as P^{30} are the result of applying the endpoint corrections on the basis of a 3.30 Mev endpoint. From the result of these corrections, it can be seen that a weaker second beta group may be overlooked if its endpoint lies near the endpoint of the stronger group.

Sulfur 31

S^{31} was formed by a (γ, n) reaction on S^{32}. The target was pressed sulfur powder. All of the recordings were made with the beam at 65 Mev, the bombard and record time at five seconds, and the record delay at one second. Figures 15 and 16 are the spectrum and Kurie plot obtained for one of the runs. In addition to the endpoints recorded for S^{31}, there was another activity formed with an endpoint of 3.3 Mev. The recorded

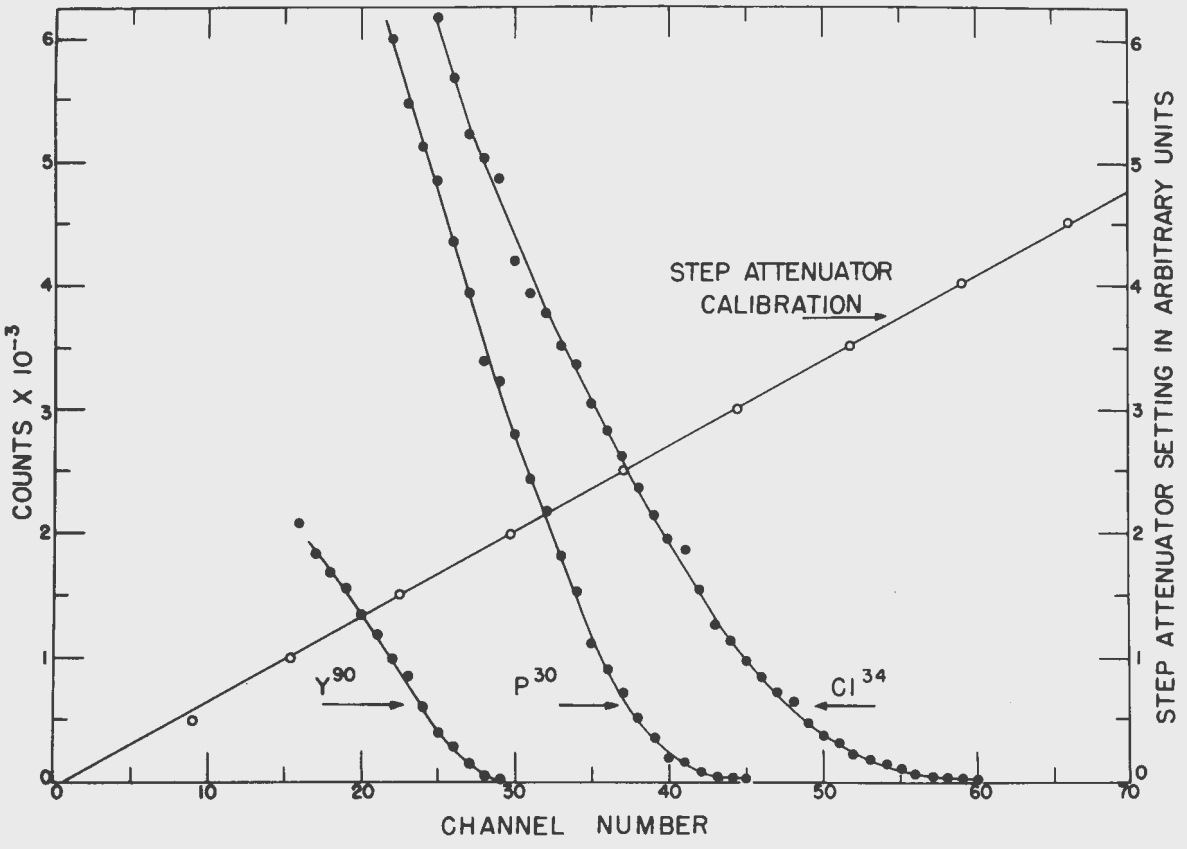

Figure 11. Beta Spectra of P^{30}, Cl^{34}, and Y^{90}

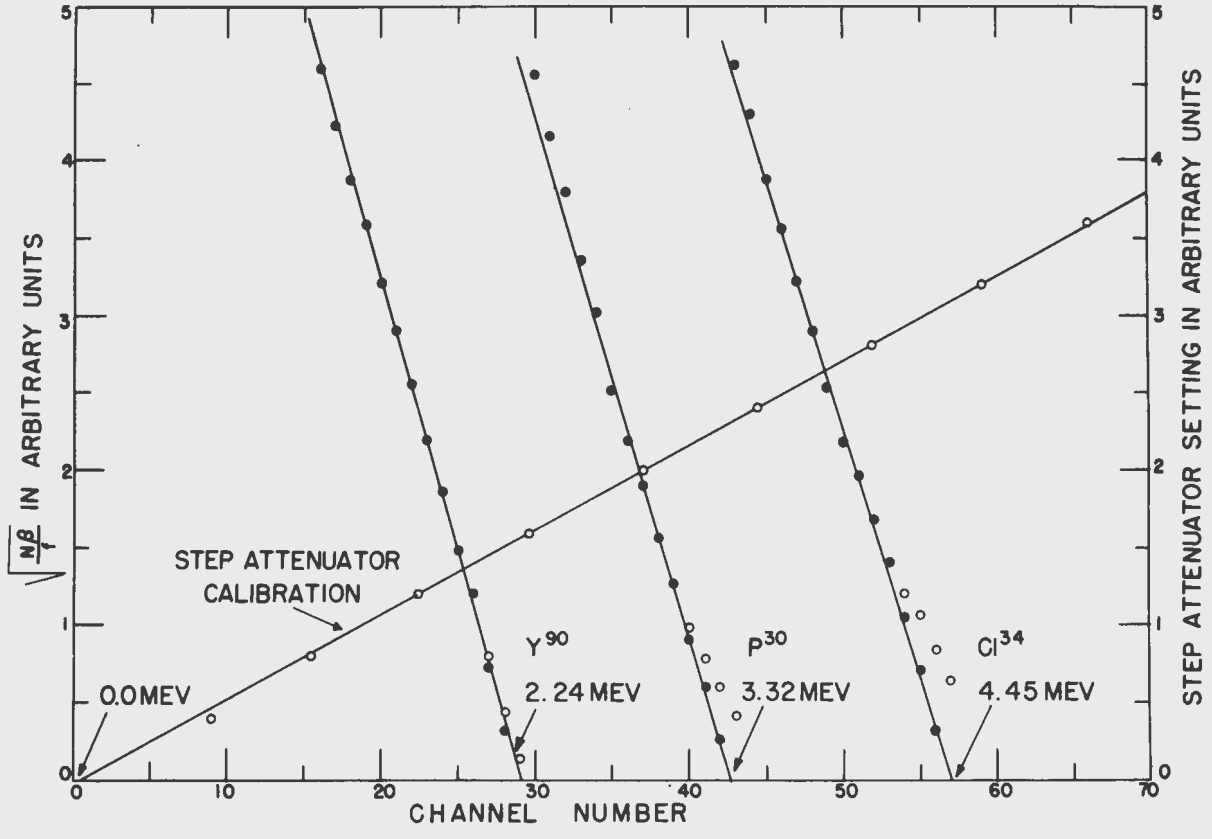

Figure 12. Kurie Plots of P^{30}, Cl^{34}, and Y^{90}.

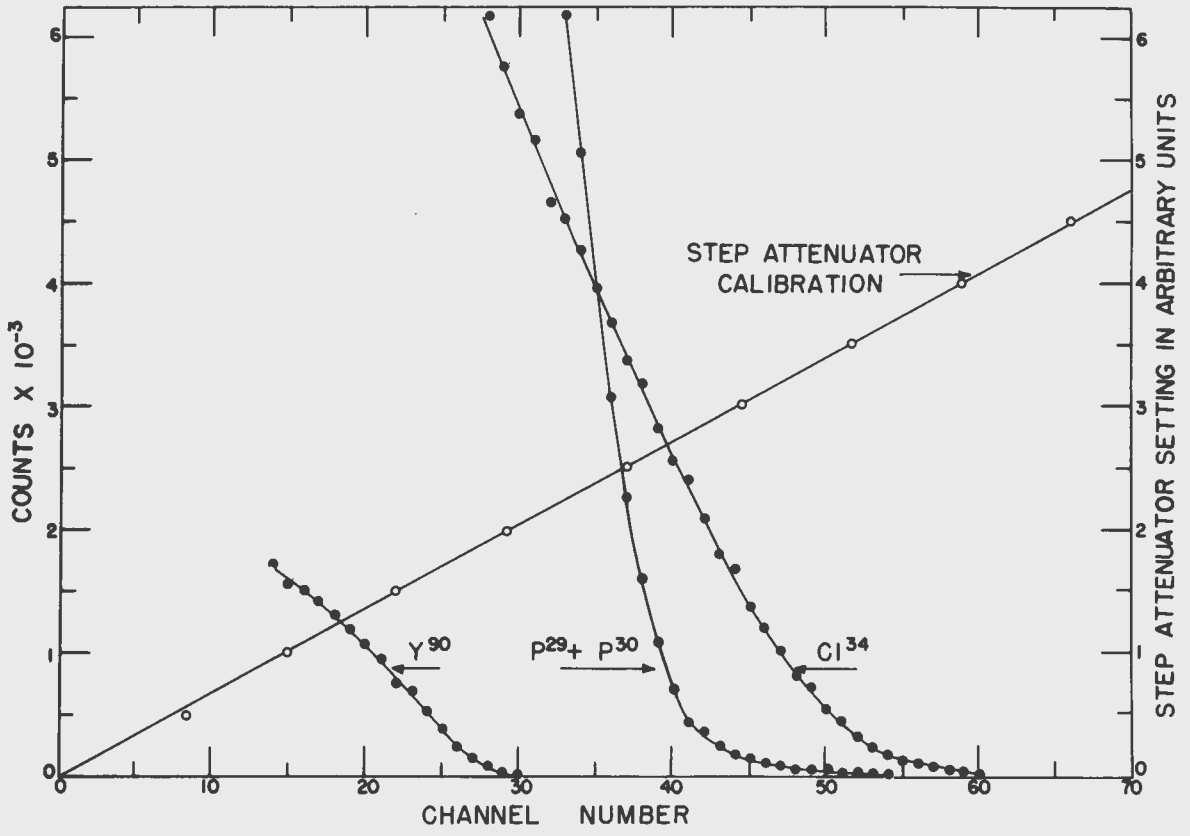

Figure 13. Beta Spectra of P^{29} + P^{30}, Cl^{34}, and Y^{90}

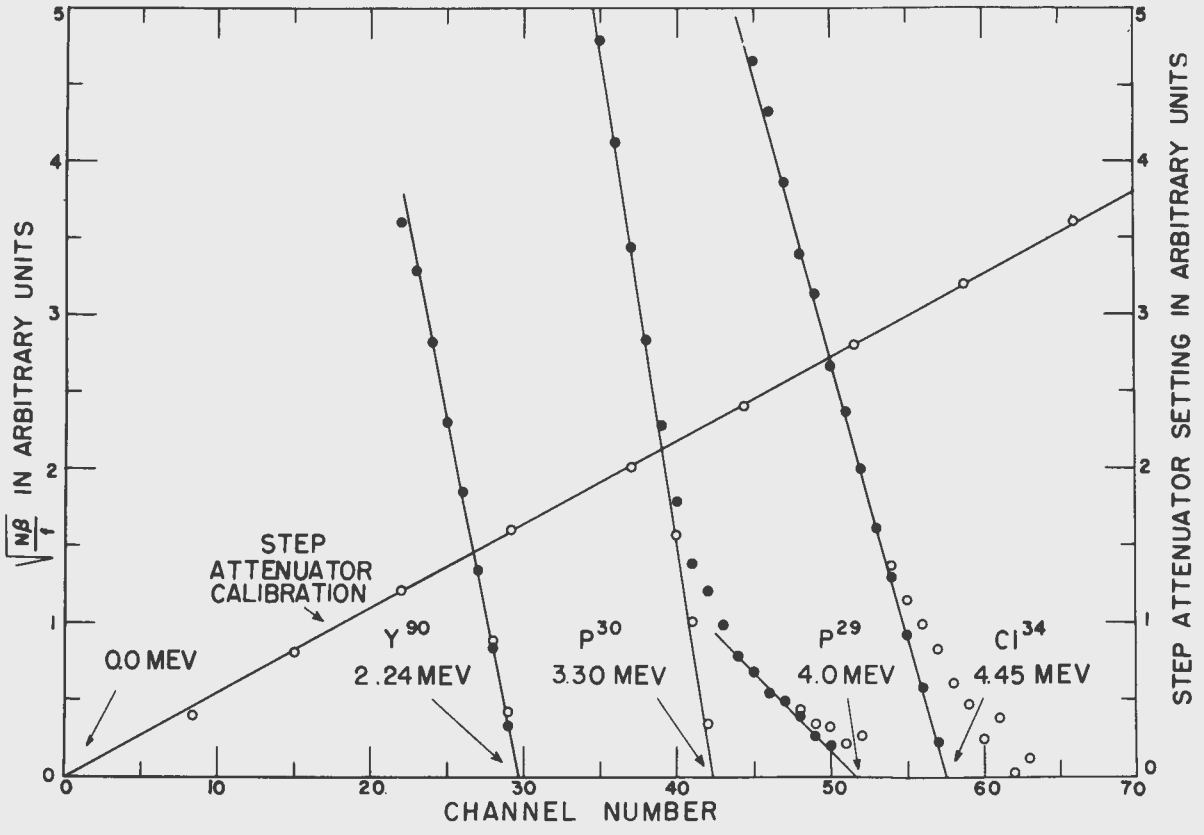

Figure 14. Kurie Plots of P^{29} + P^{30}, Cl^{34}, and Y^{90}.

intensity of this group as compared to the higher energy group was estimated to be about one to two for the 65 Mev bombardments. This activity seemed to be long lived as compared to the cycle duration, and when measured by Kline (33), a half-life in agreement with the 2.5 minute half-life of P^{30} was obtained. This agrees with the discussion in Silicon 27 regarding the amount of the (γ,pn) and (γ,d) reactions as compared to the (γ,n).

Kofoed-Hansen predicts a half-life of 1.8 seconds and a maximum beta energy of 4.19 Mev for S^{30}. With the cycle times used and the low initial production of S^{30} expected, the S^{30} should not be evident over the background of S^{31}. If any was observed, it could not be separated from the bending of the Kurie plot caused by the loss of high energy electrons through the edge of the crystal. Since Phipps found a 2.40 $\pm$ 0.07 second half-life in S^{31}, the principal beta group was assigned to this isotope.

The two runs with the Cl^{34} calibrations were assigned most of the weight in determining the 4.50 $\pm$ 0.10 Mev endpoint value for S^{31}, because the S^{31} endpoint value was very close to the Cl^{34} endpoint value.

The value of 4.50 $\pm$ 0.10 Mev is in considerable disagreement with the value of 4.06 $\pm$ 0.20 Mev by Boley and the two cloud chamber measurements of 3.85 $\pm$ 0.07 (34) and 3.87 $\pm$ 0.15 Mev (35). The second beta group with an endpoint energy of 3.3 Mev may have led Boley to assume too low an endpoint for endpoint corrections. An extrapolation of the middle portion of the Kurie plot until it crossed the energy axis gave a value of about 4.0 Mev.

Chlorine 33 and 34

The targets for both the Cl^{33} and the Cl^{34} were made of pressed NH_4Cl. The Cl^{34} calibration target was unmounted, but the target for the three attempts to measure Cl^{33} was mounted in the usual manner. The synchrotron was run at 65 Mev maximum beam energy and the cycling equipment was set to bombard four seconds and to record four seconds after a delay of from one-half to one second. A short half-life was observed and recorded. Only one beta group with an endpoint of 4.45 $\pm$ 0.10 Mev was observed. This is in agreement with the work of Arber and Stahelin (36) which showed that the 1.58 second triplet isotopic spin state of Cl^{34} decays with a 4.45 Mev maximum beta energy.

The masking of the $(\gamma,2n)$ reactions by the (γ,n) reactions is in agreement with the assignments in other parts of this work and is, also, in agreement with the findings of Edwards and MacMillan that the relative yields of the reactions are probably of the order of one to ten, respect-

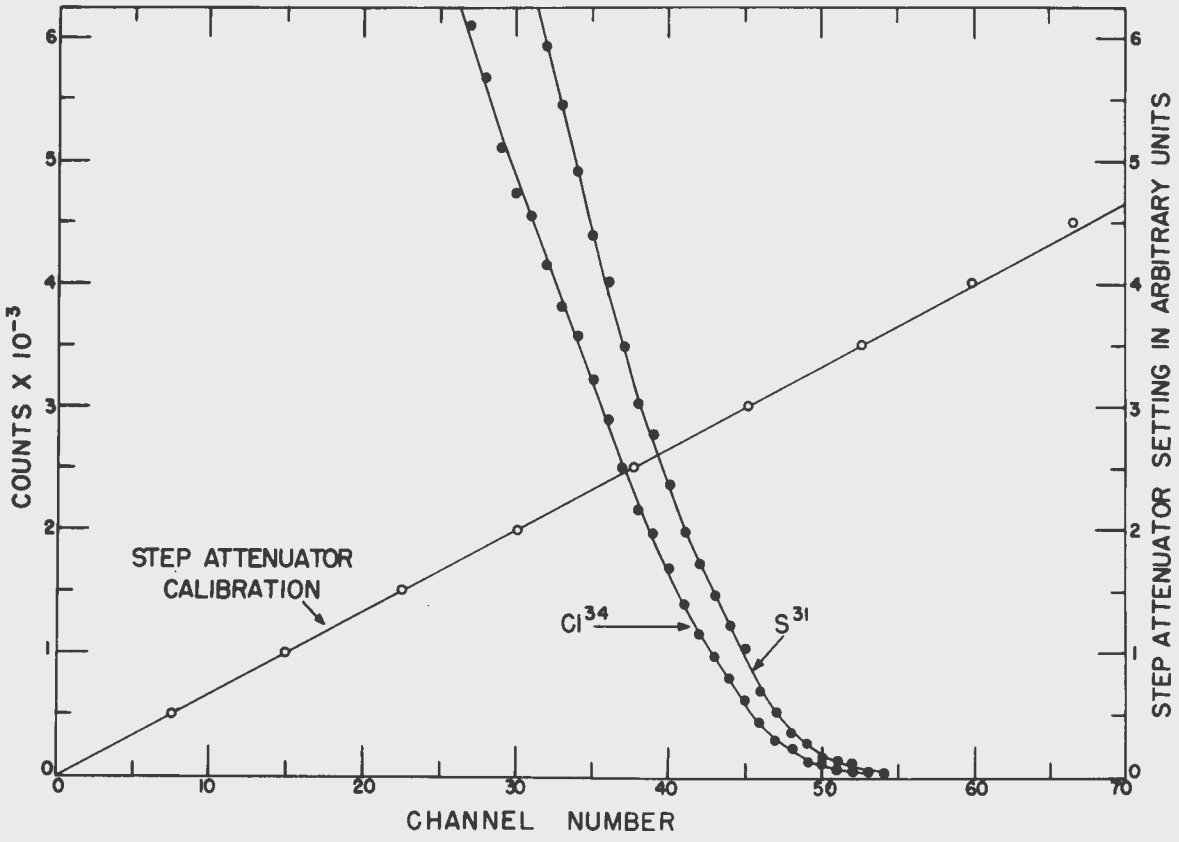

Figure 15. Beta Spectra of S^{31} and Cl^{34}.

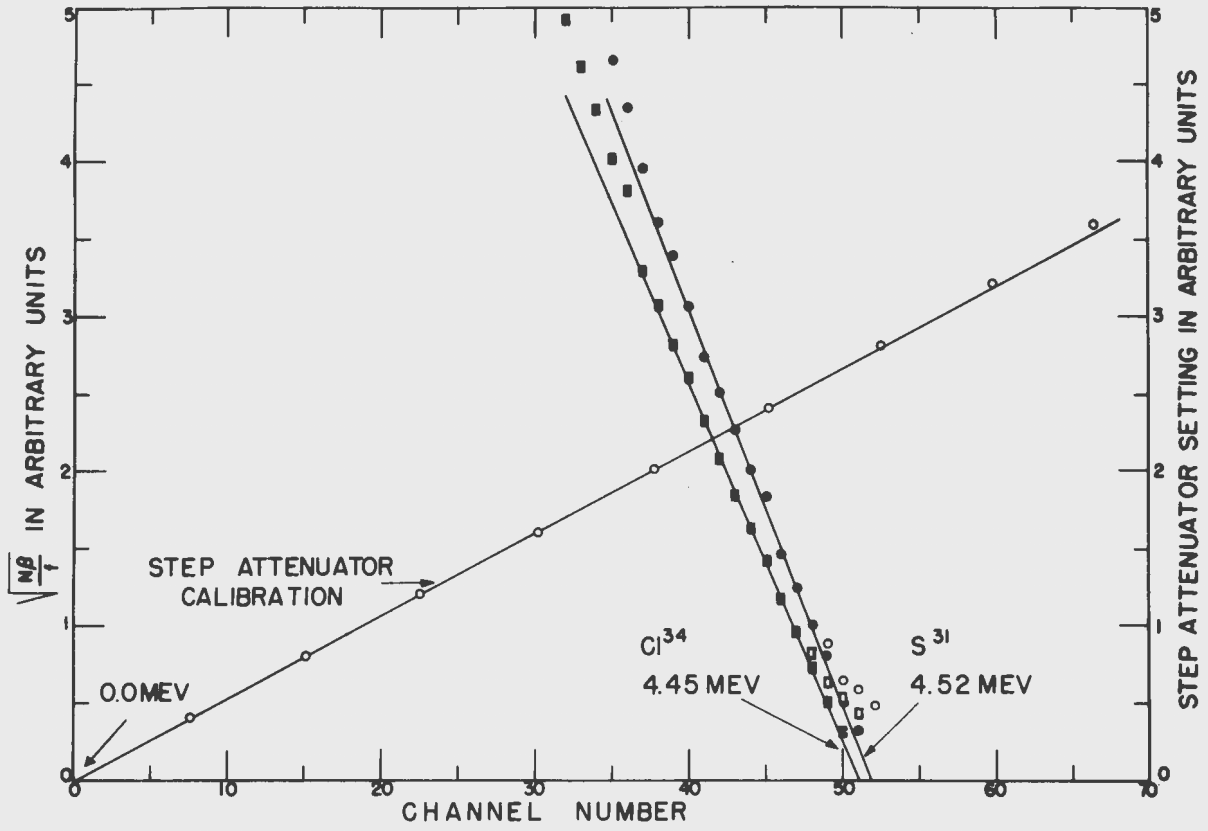

Figure 16. Kurie Plots of S^{31} and Cl^{34}.

ively. This would be further decreased due to the delay before recording if the half-life of Cl^{33} were shorter than that of Cl^{34}.

Potassium 38

The targets were made of KI for three of the runs. The target for the other run was made of KF. These were pressed powder wafers which were mounted as described earlier. The targets were bombarded for two seconds and recorded for two seconds after a delay of about one-half second with the exception of the 5.10 Mev Y^{90} determination which was bombarded for six seconds and counted for six seconds after a delay of about one second.

The intention in bombarding KI was to produce K^{37} which was reported by Phipps (10), Boley (2), and Langmuir (37) to have a half-life of about one second. The value by Phipps of 0.98 $\pm$ 0.02 seconds is considered the best of these measurements. KI was bombarded and a half-life of about one second was observed. This was recorded and the endpoint was determined to be 5.06 $\pm$ 0.11 Mev. Figures 17 and 18 show the spectrum and Kurie plot of one of the determinations. The values of the five determinations agree within experimental error. In determining the assigned endpoint value of 5.06 Mev the endpoint values determined by the Y^{90} was assigned half the weight of the values determined by the Cl^{34} calibration.

There are several reasons for assigning the 5.06 Mev value to K^{38} rather than to K^{37}. Stahelin's (38) recently reported half-life of 0.95 $\pm$ 0.03 seconds together with Kofoed-Hansen's expected half-life of 0.9 seconds and maximum beta energy of 4.84 Mev agree very well with this assignment of 5.06 Mev to K^{37}. Neither Phipps, Boley, nor Langmuir reported an attempt to determine if the half-life which they reported could be produced below the $(\gamma,2n)$ threshold. Because of the thin samples and the decrease in the beam intensity as the energy was lowered, it was not possible to run the synchrotron below the $(\gamma,2n)$ threshold and to produce enough activity to record.

Stahelin and Kofoed-Hansen state that the one second half-life of K^{38} belongs to the triplet isotopic spin state and the 7.7 minute half-life to the singlet state. Since the triplet and singlet states are expected not to differ much in energy, as in the case of Cl^{34}, the 5.06 Mev assignment is in good agreement with the 2.8 Mev beta group plus the 2.16 Mev gamma-ray. The 7.7 minute K^{38} probably decays by beta emission to the 2.16 Mev excited state of A^{38} which decays by gamma emmision.

Kofoed-Hansen predicts that if the isotopic spin is a "good quantum number", the ft values would be expected to be the same for all similar

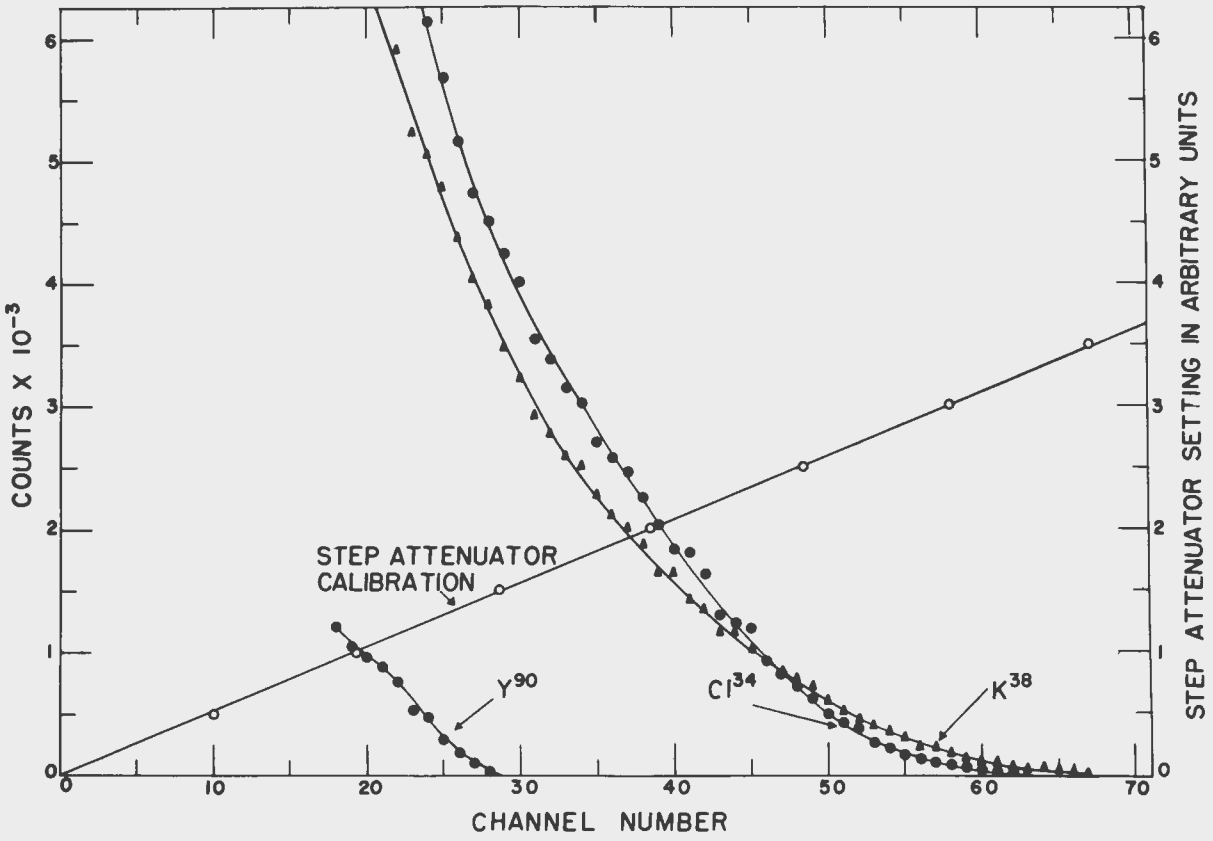

Figure 17. Beta Spectra of K^{38}, Cl^{34}, and Y^{90}.

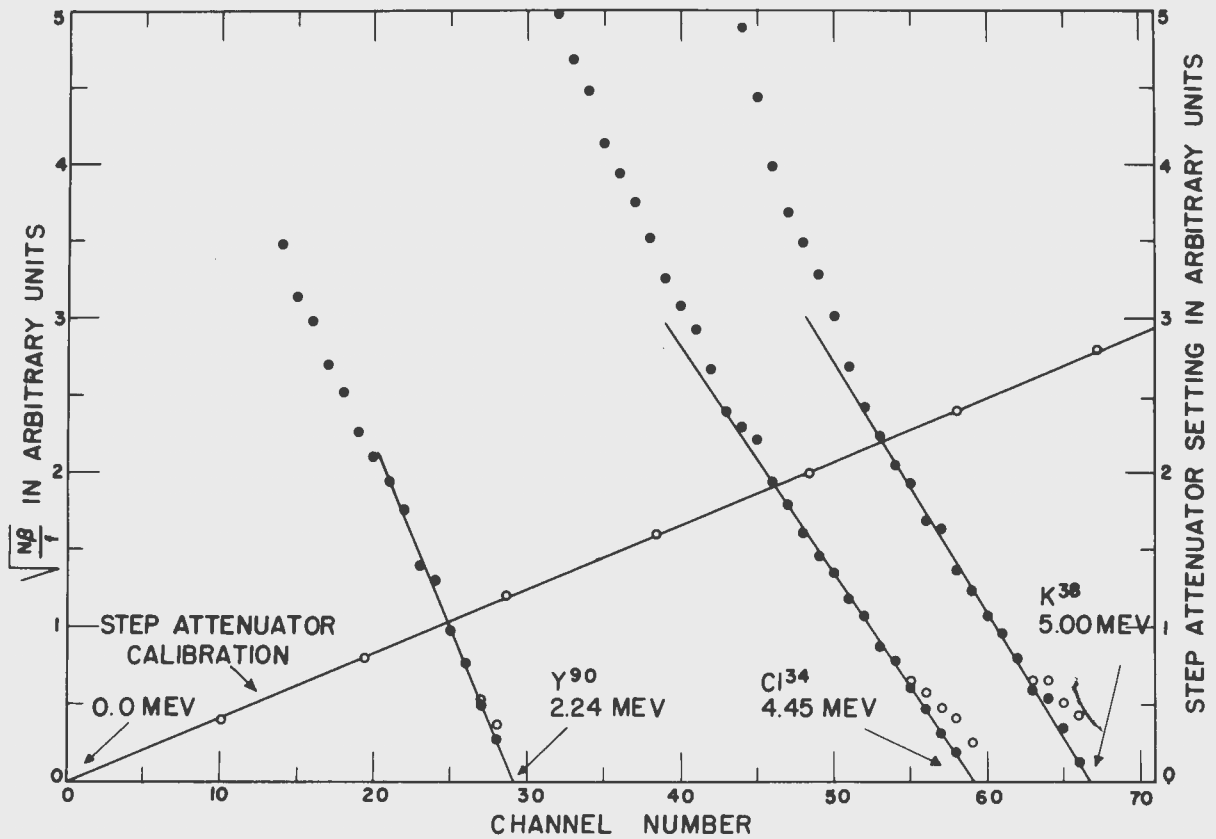

Figure 18. Kurie Plots of K^{38}, Cl^{34}, and Y^{90}

transitions. The ft value of 3300 ± 400 for K^{38} is in good agreement with the values of 3300 ± 900 for O^{14} (39) and 3000 ± 400 for Cl^{34}.

The work of Edwards and MacMillian indicates that the ratio of K^{37} to K^{38} produced should be about one to ten. There was some evidence of a second weaker beta group with an endpoint energy of 3.9 ± 0.2 Mev. In the three cases in which the bombard time and record time were about two seconds and the delay before recording about one-half of a second, estimates of the recorded intensities of the two groups gave ratios of about one to five. When the six second bombard, one second delay, and six second record cycle was run, the ratio of the recorded intensities was about one to two. This indicates that the 3.9 Mev group is longer lived than K^{38} and is probably due to K^{37}. Besides being the strongest activity recorded another indication that the 5.06 Mev beta group belongs to K^{38} was obtained from the calcium bombardment. A second beta group of 5.05 Mev was found in calcium. The ratios of the recorded intensities in calcium of the 5.05 Mev to the 6.10 Mev group was about one to two for the 65 Mev bombardments and about one to four for the 40 Mev bombardment. Also, since no gamma-ray lines of the intensities necessary for the 5.05 Mev group were observed in calcium, the 5.05 Mev group is assumed to be caused by a reaction other than the (γ,n) reaction.

If Boley actually measured a mixture of K^{37} and K^{38}, he would have probably assumed an endpoint of about 4.5 Mev on which to base his resolution corrections and would get fairly good agreement with his data.

Calcium 39

The target was made of pressed CaF powder. Ca^{39} was produced by a (γ,n) reaction on Ca^{40}. The Ca^{39} spectrum was recorded four times, of which three were at 65 Mev maximum beam energy and the fourth at 40 Mev maximum beam energy. Two of these runs and their Kurie plots are shown as Figures 19, 20, 21, and 22. Figures 21 and 22 show the linearity check which was obtained on the crystal and photomultiplier tube by running the Li^8 spectrum. This permitted, in addition to the linearity check, a determination of the Ca^{39} and a check on the 13.4 Mev endpoint of Li^8. The Li^8 was produced by a (γ,p) reaction on Be^9 which was in the form of 0.005 inch foil attached to one of the nickel and balsa holders.

Since the 6.10 Mev value was the best determination, 6.10 ± 0.11 Mev was chosen as the endpoint value of Ca^{39}. The two lower values are not considered to be as accurate as the two upper values. This is because for one of the determinations, the calibration was only by Y^{90}; and for the other, Figure 22, the scale was such that only the last four points of the Kurie plot determined the endpoint. The upper two values were both obtained by Cl^{34} and Y^{90} calibrations.

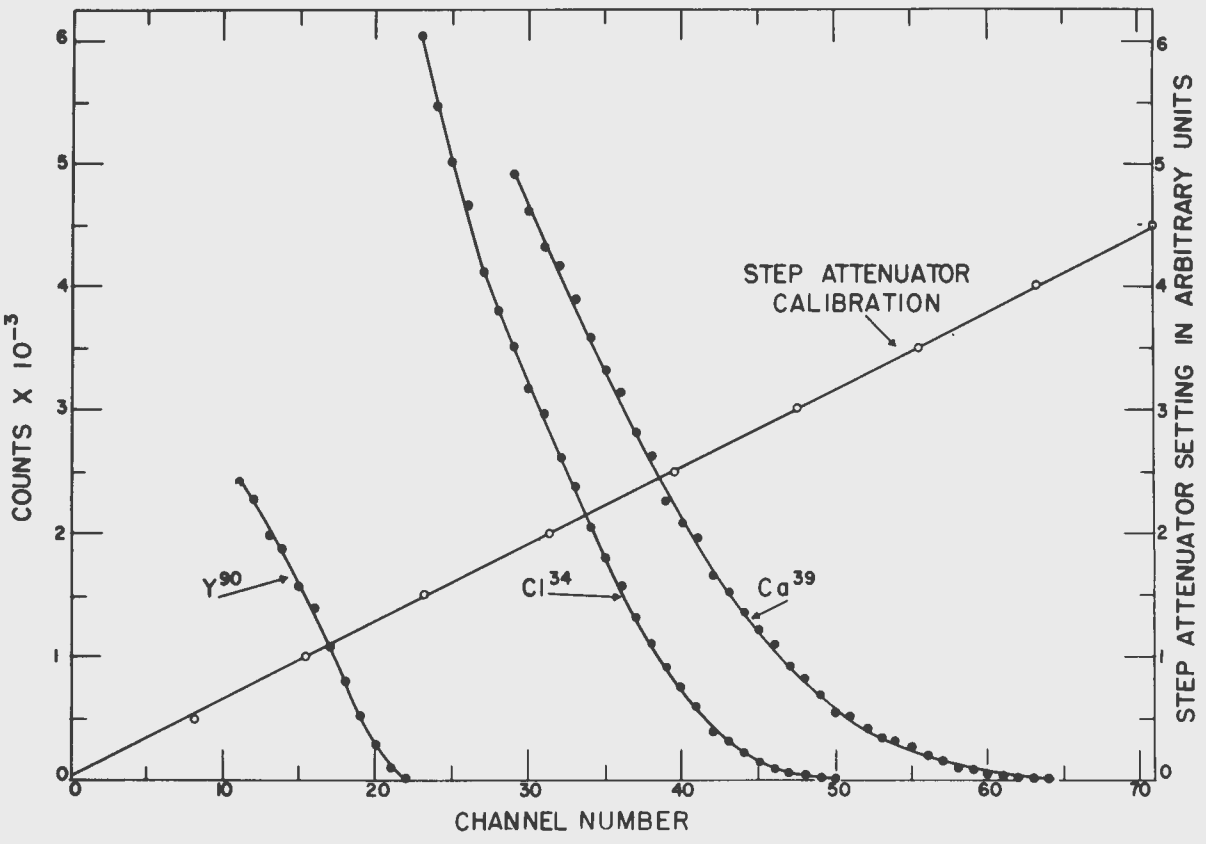

Figure 19. Beta Spectra of Ca^{39}, Cl^{34}, and Y^{90}.

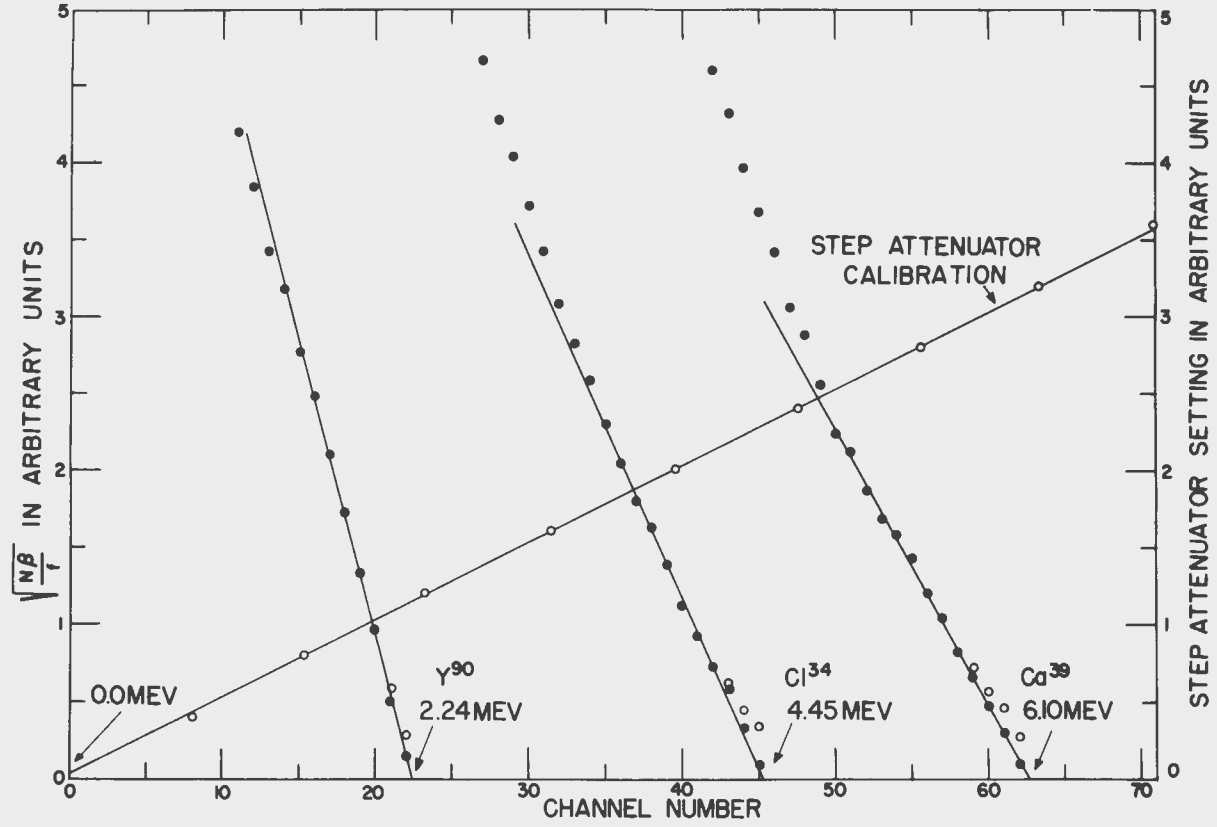

Figure 20. Kurie Plots of Ca^{39}, Cl^{34}, and Y^{90}.

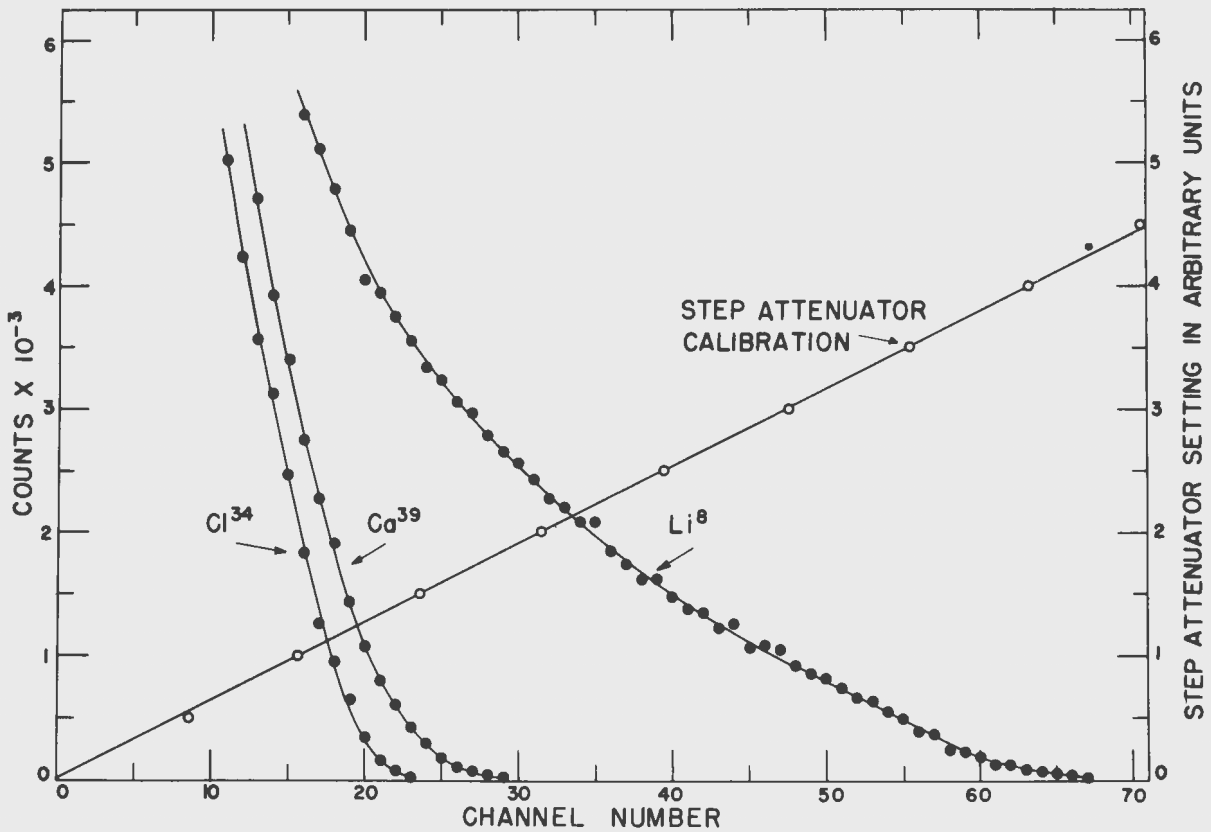

Figure 21. Beta Spectra of Ca^{39}, Li^{8}, and Cl^{34}.

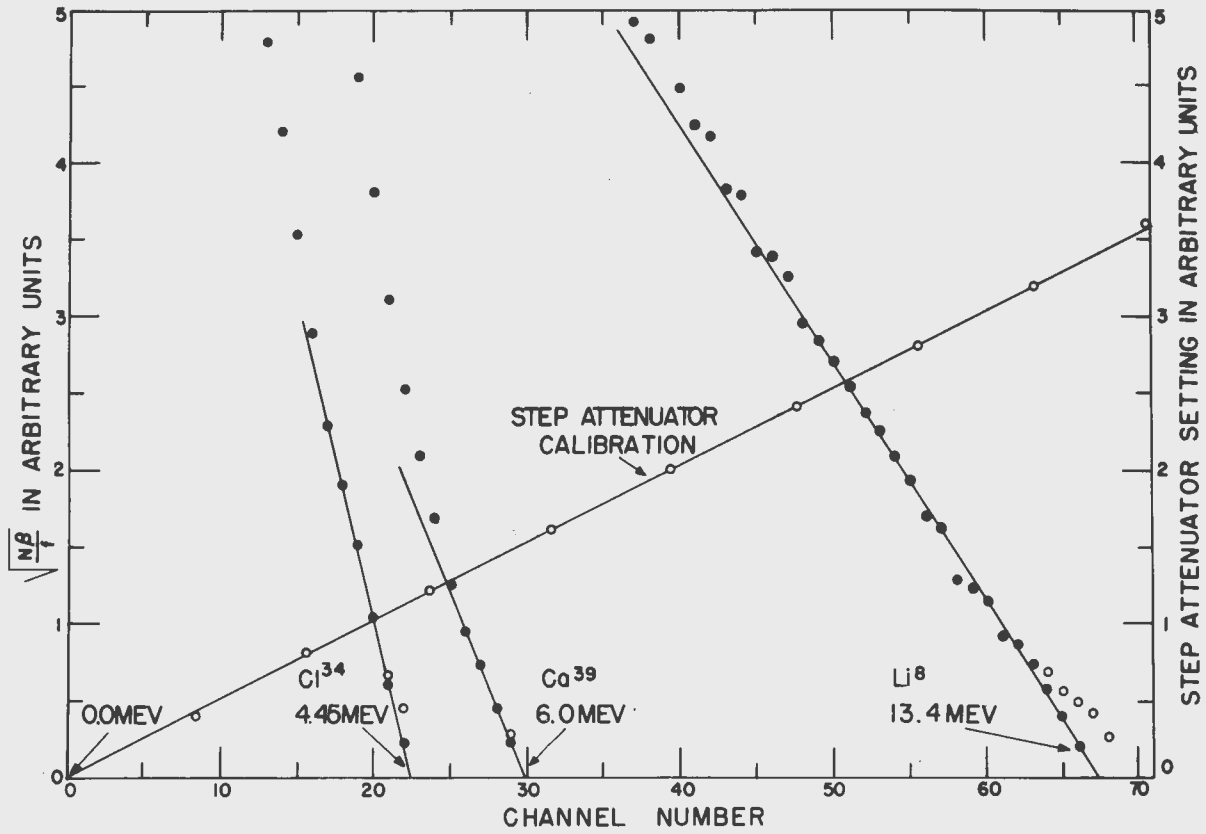

Figure 22. Kurie Plots of Ca^{39}, Li^{8}, and Cl^{34}.

The value of 6.10 ± 0.15 Mev disagrees both with Boley's value of 5.13 ± 0.20 Mev and Bramms and Smith's value of 6.7 ± 0.5 Mev (40). The latter value was determined by absorption techniques. The difference between the value reported here for Ca^{39} and Boley's value can be explained by the second beta group, discussed under Potassium 38 which Boley was unable to detect with his equipment. The number of channels for calcium in Figures 21 and 22 is about the same as used in Boley's determination. Since he had a reported 44 per cent resolution for the 624 kev Cs^{137} line, the bends in the Kurie plot would have been obscured and attributed to resolution spread. This would have led him to assume too low an endpoint for resolution corrections and thereby obtain too low a value.

According to Kofoed-Hansen, Ca^{38} should have a half-life of 0.7 seconds and a maximum beta energy of 5.21 Mev. This half-life and energy are not much different than those for K^{38}. The amount of Ca^{38} produced as compared to the amount of K^{38} is probably about one to two for the 65 Mev bombardments. Because of the delay of about 0.5 seconds between bombarding and recording, the amount of Ca^{38} recorded as compared to the amount of K^{38} recorded would be reduced by another factor of about two.

Since the second beta group's endpoint of 5.05 Mev agreed with the endpoint assigned to K^{38} and since the intensity of the 5.05 Mev beta group as compared to the 6.10 Mev beta group was reduced by a factor of two when the maximum bombarding energy was reduced, the 5.05 Mev energy was assigned to K^{38} and the 6.10 value to Ca^{39}.

Gamma-rays

In order to determine that the other beta groups were not caused by another branch in the decay process, the activities investigated were searched for gamma-rays. The results of this search indicate that if branching does occur, it occurs in such small amounts that it would not show in the beta spectra in this investigation.

The gamma-ray sources were prepared by filling a nickel box with the material to be bombarded. The box was made the size of the balsa block so that the same transport system could be used. This permitted the NaI(Th) crystal, which was used for recording the gammas, to be placed in a position where it would not be activated by the X-ray beam from the synchrotron. About 0.5 inches of aluminum absorber were placed between the target and the crystal. This was sufficient to stop the expected beta-rays.

Two methods were used in this part of the investigation. The first was to bombard the target and to take still pictures. The results, which were also visible on the oscillograph, gave the expected intense line at

0.51 Mev and the Compton edge resulting from it. Since only one beta group was observed with an endpoint within 0.5 Mev of the reported endpoints, and since there was no evidence of any strong gamma-ray lines with energy less than 0.5 Mev besides that due to the annihilation radiation, no further investigations were carried out in this region.

In order to determine if the second beta groups observed were accompanied by gamma rays, the following procedure was used. Instead of taking photographs of the spectra, the number of gamma-rays with energies above the annihilation peak was compared to the total number with energies above some fixed value in the neighborhood of 0.2 Mev. This was accomplished in the following manner. The equipment for recording was set up as described for the photographs except that, instead of taking pictures, the pulses from the amplifier were fed into a discriminator which, if fired, produced a pulse that was counted by a scaler. The discriminator used was a single channel differential analyzer, of the Oak Ridge type, used in the integral position. With the gain control on the amplifier turned to the lowest of ten fixed positions which resulted in an attenuation of about three times, the discriminator was set just above the annihilation peak. This was checked by observing that it passed the Cs^{137} 0.66 Mev gamma-ray. When the gain of the amplifier was turned to its maximum position, pulses of about 0.2 Mev were passed.

The cycling equipment was operated such that the sample was bombarded and then counted for a few cycles. If no background was being built up, the runs were averaged and the figures were rounded off to the values shown in Table 2. Runs were made with the amplifier gain set at minimum and maximum, with and without the target, resulting in four sets of data for each bombardment energy. Trial runs on magnesium were made at various bombardment energies. Due to the low intensity of the sychrotron X-ray beam at low energies, it was necessary to raise the beam energy to 30 Mev before a usable amount of activity could be produced. Runs were made at 30 and 35 Mev maximum beam energy. Table 2 gives the results of these runs.

The background for all the similar runs without a target was averaged to give the gamma-ray background in the room. If the backgrounds are subtracted from the appropriate columns, an estimate of the ratio of gamma-rays above 0.6 Mev to those above 0.2 Mev can be obtained. For the 35 Mev bombardments the ratio is the order of two per cent in each case. Since these values represented integrated spectra, it can be concluded that if branching occurs with the emission of a gamma-ray of greater than 0.6 Mev energy, the intensity of these transitions is very small as compared to the annihilation radiation intensity. A further conclusion is that the second beta groups are not due to branching since the intensities would be so low that they would not record.

Table 2. Results of Counting the Integrated Gamma-ray Spectra.

Target	Bomb. Time (sec)	Record Time (sec)	Beam Energy (Mev)	Counts with Target Amplifier Gain Max.	Min.	Counts without Target Amplifier Gain Max.	Min.
Mg	18	23	30	5500	470	1100	300
Mg	18	23	35	11100	510	1150	310
LiCl	3	5	30	1100	65	190	50
LiCl	3	5	35	2000	90	190	50
S	3	5	30	1200	75	190	50
S	3	5	35	3200	110	190	50
Si	3	5	30	1650	90	190	50
Si	3	5	35	3900	140	190	50
KI	3	3	30	550	60	150	25
KI	3	3	35	1100	70	150	25
P	5	5	30	No appreciable activity above phosphorous 30 background.			
P	5	5	35	4000	110		
Ca	5	5	30	1300	85	200	50
Ca	5	5	35	2750	120	200	50
Ni box	5	5	30	220	50	200	50
Ni box	5	5	35	230	50	200	50

IV. SUMMARY AND CONCLUSIONS

A comparison of the results of this investigation and those of others is principally a comparison of this work and that of Boley and Zaffarano. Because of the lage differences in some of the reported values and the values reported here, each spectrum in question was repeated several times, sometimes months apart, in order to assure that the results were not caused by some unknown change in the recording equipment between the time the calibration was placed on the film and the unknown spectrum was recorded.

Boley's dot spectra were counted by eye on a microfilm viewer. It was not practical to have many channels or to count large numbers of events. The number of channels along the straight portion of his Kurie plots varied between six and nine. Because of the 44 per cent resolution at 624 kev, three of four of these channels were corrected for

resolution effect of endpoint corrections. As mentioned earlier, the endpoint corrections have the effect that if the endpoint is assumed too low, the corrections tend to make the corrected points agree with the assumption.

The endpoint energies obtained in this investigation and the best known values of the half-lives are combined in Table 3 to give the ft values.

With the exception of K^{38} and Cl^{34}, the ft values increase as the atomic number increases. This indicates that the ft value assigned to K^{38} does not seem to belong to the mirror nuclei, but to the triplet

Table 3. Beta Endpoint Energies and ft Values Obtained in This Investigation.

Nuclei	E_{max}	$t_{\frac{1}{2}}$ (sec)		ft (sec)
Mg^{23}	2.95 ± 0.07	10.7 ± 0.7	(10)	3600 ± 500
Si^{27}	3.76 ± 0.08	4.05 ± 0.10	(10)	4000 ± 450
S^{31}	4.50 ± 0.10	2.40 ± 0.07	(10)	5250 ± 600
Cl^{34}	4.45 ± 0.10	1.58 ± 0.05	(38)	3000 ± 400
K^{38}	5.06 ± 0.11	0.95 ± 0.03	(38)	3250 ± 400
Ca^{39}	6.10 ± 0.15	0.90 ± 0.05	(33)	7150 ± 1000
P^{30}	3.31 ± 0.07	150	(27)	

isotopic spin state where the Fermi interaction form, $|\int 1|^2$, probably has the value of two (26) instead of one as in the case of the mirror nuclei. Doubling the ft values for K^{38} and Cl^{34} brings them into agreement with the trend of the other ft values.

The ft values, combined with the values of $|\int \sigma|^2$ derived by Winther and Kofoed-Hansen do not lead to their unique value for the ratio of G - T to Fermi interaction strength constants, which they obtained by using previous data.

Since improved equipment is being developed, these activities should be examined again for second beta groups and for better endpoint determinations. The endpoints should be re-run if enough activity can be produced below the (γ,d) threshold to record.

Further investigations should be made for gamma-rays, especially below 0.51 Mev.

V. BIBLIOGRAPHY

1. W. A. Hunt, W. Rhinehart, J. Weber, and D. J. Zaffarano, Ames Laboratory Report, ISC-359 (1953); submitted to the Rev. Sci. Instr. for publication.

2. F. I. Boley and D. J. Zaffarano, Phys. Rev. 84, 1059 (1951) and references contained in Ames Laboratory Report, ISC-154 (1951) by the same authors.

3. E. J. Konopinski, Revs. Modern Phys. 15, 209 (1943).

4. E. Fermi, Z. Physik 88, 161 (1934).

5. G. Gamow and E. Teller, Phys. Rev. 49, 895 (1936).

6. E. Wigner, Phys. Rev. 51, 947 (1937); Phys. Rev. 56, 519 (1939).

7. S. Moszkowski, Phys. Rev. 82, 118 (1951).

8. G. L. Trigg, Phys. Rev. 86, 506 (1952).

9. A. Winther and O. Kofoed-Hansen, Dan. Mat. Fys. Medd. 27, no. 14 (1953).

10. P. L. Phipps, The Half-lives of Some Short Lived Low Z Nuclei formed by Photonuclear Reactions, Unpublished M. S. Thesis, Ames, Iowa State College Library. (1953).

11. J. M. Hollander, I. Perlman, and G. T. Seaborg, Revs. Modern Phys. 25, 483 (1953).

12. L. Ruby and J. R. Richardson, Phys. Rev. 83, 659 (1951).

13. W. F. Hornyak and T. Lauritsen, Phys. Rev. 77, 160 (1950).

14. J. B. Birks, Scintillation Counters, N.Y., McGraw-Hill Book Co.,Inc. 1953.

15. L. J. Laslett, E. N. Jensen, and A. Paskin, Phys. Rev. 79, 412 (1950).

16. J.P. Palmer and L. J. Laslett, Ames Laboratory Reports, AECU-1220 (1951) and ISC-174 (1950).

17. L. Szilard and T. A. Chalmers, Nature (London) 134, 462, 494 (1934).

18. J. Moreau and J. Perez y Jorba, Comp. rend. 235, 38 (1952).

19. C. M. Braden, L. Slack, and F. B. Schull, Phys. Rev. 75, 1964 (1949).

20. L. J. Laslett, E. N. Jensen, and A. Paskin, Phys. Rev 79, 412 (1950).

21. E. N. Jensen and L. J. Laslett, Phys. Rev. 75, 1949 (1949).

22. L. M. Langer and H. C. Price, Jr., Phys. Rev. 76, 641 (1949).

23. E. N. Jensen and T. Nichols, Ames, Iowa, (Private communication) 1953.

24. M. G. White, L. A. Delsasso, J. G. Fox, and E. C. Creutz, Phys. Rev. 59, 63 (1941).

25. L. S. Edwards and F. A. MacMillian, Phys. Rev. 87, 377 (1952).

26. O. Kofoed-Hansen, Phys. Rev. 92, 1075 (1953).

27. F. I. Boley, Short Lived Synchrotron Induced Activities. Unpublished Ph.D. Thesis, Ames, Iowa, Iowa State College Library. (1950).

28. W. H. Barkas, E. C. Creutz, L. A. Delsasso, and R. A. Sutton, Phys. Rev. 61, 106 (1942).

29. R. L. McCreary, G. Kuerti, and S. N. Van Voorhis, Phys. Rev. 57, 351 (1940)(A).

30. H. Roderick and C. Wong, Phys. Rev. 92, 204 (1953).

31. C. Mangnan, Ann. phys. 15, 5 (1941).

32. E. Bleuler, W. Zunti, Helv. Phys. Acta 19, 375 (1946).

33. R. Kline, Ames, Iowa, Preliminary investigation, (Private communication) 1953.

34. M. G. White, E. C. Creutz, L. A. Delsasso, and R. R. Wilson, Phys. Rev. 59, 63 (1941).

35. D. R. Elliott and L. D. P. King, Phys. Rev. 59, 403 (1941).

36. W. Arber and P. Stahelin, Helv. Phys. Acta 26, 433 (1953).

37. R. V. Langmuir, Phys. Rev. 74, 1559 (1948) (A).

38. P. Stahelin, Phys. Rev. 92, 1076 (1953).

39. F. Ajzenberg and T. Lauritsen, Revs. Modern Phys. 24, 321 (1952).

40. R. Braams and C. L. Smith, Phys. Rev. 90, 995 (1953).

41. E. Feenberg and G. Trigg, Revs. Modern Phys. 22, 399 (1950).

42. S. A. Moszkowski, Phys. Rev. 82, 35 (1951).

VI. APPENDIX

An estimate of the relative intensities of two beta groups separated by the usual subtraction process with a Kurie plot can be made from the two slopes observed near the endpoint energies. From the Fermi theory of beta decay, it is evident that the ratio of the number of events in each group will be given by

$$\frac{N_2}{N_1} = \left[\frac{T_2}{T_1} \right]^2 \frac{f_2}{f_1}$$

where the subscripts 1 and 2 refer to the first and second beta groups, respectively, N is the total number of events, T is the observed slope, and f is the dimensionless integral,

$$f = \int_1^{E_o} F(E,Z)(E^2-1)^{\frac{1}{2}} E(E_o-E)^2 dE,$$

which has been evaluated and presented graphically by Feenberg and Trigg (41) and Moszkowski (42) for the allowed transitions.*

The use of the above relation for the relative intensities involves the assumption that the beta spectrum observed with a scintillation spectrometer is not appreciably affected near the endpoint by the degradation of the energy spectrum caused by the electrons scattering out of the highest energy third of the spectrum, as demonstrated by Figures 4 and 6.

---

*The terms in the latter equation have been defined in Chapter I.